Trinity University
Digital Commons @ Trinity

Geosciences Faculty Research | Geosciences Department

3-1997

Enclaves in the Cadillac Mountain Granite (Coastal Maine): Samples of Hybrid Magma from the Base of the Chamber

R. A. Wiebe

Diane R. Smith
Trinity University, dsmith@trinity.edu

M. Sturm

E. M. King

M. S. Seckler

Follow this and additional works at: https://digitalcommons.trinity.edu/geo_faculty

Part of the Earth Sciences Commons

Repository Citation
Wiebe, R.A., Smith, D.R., Sturm, M., King, E.M., & Seckler, M.S. (1997). Enclaves in the Cadillac mountain granite (coastal Maine): Samples of hybrid magma from the base of the chamber. *Journal of Petrology, 38*(3), 393-423. doi:10.1093/petroj/38.3.393

This Article is brought to you for free and open access by the Geosciences Department at Digital Commons @ Trinity. It has been accepted for inclusion in Geosciences Faculty Research by an authorized administrator of Digital Commons @ Trinity. For more information, please contact jcostanz@trinity.edu.

JOURNAL OF PETROLOGY | VOLUME 38 | NUMBER 3 | PAGES 393–423 | 1997

Enclaves in the Cadillac Mountain Granite (Coastal Maine): Samples of Hybrid Magma from the Base of the Chamber

R. A. WIEBE[1*], DIANE SMITH[2], MARNIE STURM[3], E. M. KING[4] AND M. S. SECKLER[5]

[1]DEPARTMENT OF GEOSCIENCES, FRANKLIN AND MARSHALL COLLEGE, LANCASTER, PA 17604, USA

[2]DEPARTMENT OF GEOSCIENCES, TRINITY UNIVERSITY, SAN ANTONIO, TX 78212, USA

[3]DEPARTMENT OF GEOLOGY, DUKE UNIVERSITY, DURHAM, NC 27706, USA

[4]DEPARTMENT OF GEOLOGY AND GEOPHYSICS, UNIVERSITY OF WISCONSIN, MADISON, WI 53706, USA

[5]DEPARTMENT OF GEOLOGY, WILLIAMS COLLEGE, WILLIAMSTOWN, MA 01267, USA

RECEIVED JUNE 20, 1996 ACCEPTED OCTOBER 21, 1996

The Cadillac Mountain intrusive complex is dominated by the Cadillac Mountain granite and a 2–3 km thick section of interlayered gabbroic, dioritic and granitic rocks which occurs near the base of the granite. The layered rocks record hundreds of injections of basaltic magma that ponded on the chamber floor and variably interacted with the overlying silicic magma. Magmatic enclaves, ranging in composition from 55 to 78 wt % SiO_2, are abundant in granite above the layered mafic rocks. The most mafic enclaves are highly enriched in incompatible elements and depleted in compatible elements. Their compositions can be best explained by periodic replenishment, mixing and fractional crystallization of basaltic magma at the base of the chamber. The intermediate to silicic enclaves formed by hybridization between the evolved basaltic magma and resident silicic magma. There is little evidence for significant exchange between enclaves and the enclosing granite. Instead, hybridization apparently occurred between stratified mafic and silicic magmas at the base of the chamber. Enclaves in a restricted area commonly show distinctive compositional characteristics, suggesting they were derived from a discrete batch of hybrid magma. Enclaves were probably dispersed into a localized portion of the granitic magma when replenishment or eruption disrupted the intermediate layer.

KEY WORDS: *granite*; *enclaves*; *mafic–silicic layered intrusion*; *fractional crystallization*; *zoned magma chamber*

INTRODUCTION

Enclaves occur in nearly all granites and have recently been the focus of many studies [see reviews by Vernon (1983) and Didier & Barbarin (1991)]. Although enclaves may have originated in many different ways and from different sources, there has been a growing consensus that there are textural criteria to recognize a class of enclaves that formed from different magmas that were mingled into the granitic magma while it was still mobile (Vernon, 1984, 1990); these can appropriately be termed magmatic enclaves. Their compositions are commonly intermediate but can vary from basaltic to highly silicic. Magmatic enclaves occur in all types of granite and are probably the dominant type of enclave in most calc-alkaline I-type granites. In spite of partial reequilibration, enclaves of this type commonly have Nd isotopic compositions that are distinct from the enclosing granite and support their formation from mantle-derived magmas (Holden *et al.*, 1987).

The compositions of magmatic enclaves can vary widely even within a single pluton, and they can only rarely be interpreted as simple mixtures between an original basaltic magma and the host granitic magma. There is ample petrographic and chemical evidence in many enclaves for hybridization (mixing of liquids and exchange of crystals) and selective chemical and isotopic

*Corresponding author. Present address: School of Earth Sciences, Macquarie University, N.S.W. 2109, Australia.

© Oxford University Press 1997

Downloaded from https://academic.oup.com/petrology/article-abstract/38/3/393/1564739
by Trinity University user
on 15 February 2018

diffusion. Not all of this hybridization necessarily occurred between the enclave and the host granite. In volcanic studies it is commonly recognized that some hybridization must have taken place in a different setting and in a larger volume of magma (probably in a mafic to intermediate layer at the base of the chamber) before the formation of the enclave (Bacon, 1986; Stimac *et al.*, 1990). Many studies of enclaves in plutonic rocks have led to similar conclusions (Dodge & Kistler, 1990; Barbarin, 1991). Nonetheless, in plutonic rocks where slow cooling has occurred, studies of enclaves in granites have commonly focused on exchange that presumably took place between enclaves and the enclosing host granite (e.g. Bedard, 1990; Bussy, 1991; Debon, 1991; Orsini *et al.*, 1991; Blundy & Sparks, 1992; Seaman & Ramsey, 1992).

There are many factors, including relative volumes of the two magmas and temperature contrasts between them, that will affect how much time is available for exchange above or below the solidus of the enclave (Furman & Spera, 1985; Sparks & Marshall, 1986; Frost & Mahood, 1987). Significant exchange between mafic and silicic magmas is most likely to occur while both enclave and host have high proportions of liquid. This can be seen very clearly in some composite dikes where chilled pillows of basalt have rapidly solidified and then fractured during flow: along the initially quenched margins the basaltic enclave contains abundant biotite, and the adjacent granite has been strongly depleted in K_2O, whereas along fractured surfaces of the basaltic pillow (which probably formed no more than about 1 h later), there appears to be no significant exchange of alkalis (Wiebe, 1973). Here, significant exchange appears to have occurred mainly in the first few minutes of contact between the two magmas. Where enclaves preserve chilled, crenulate margins against the surrounding granite, a good case can be made that exchange between the enclave and the adjacent granite began at conditions above the enclave solidus. Where the enclaves are of uniform grain-size with simple curved or straight boundaries and no chilled margins, it is possible that the enclave was completely solid when it came into contact with the granite immediately surrounding it. The compositions of these enclaves may reflect, in many instances, hybridization that occurred at an earlier stage and at a remote location.

Although the specific sources of magmatic enclaves in a granite are rarely known, there are commonly thought to be three possibilities. The first consists of new, generally more mafic magma injected as dikes that pass from the solid margin into the liquid interior of a granitic magma chamber; these injections rapidly break up into enclaves and may be distributed by convection throughout the granite (Frost & Mahood, 1987; Pitcher, 1991). Some of these enclaves, if large enough and rapidly quenched, may have chemical and isotopic compositions which closely approach that of the injected magma. Most, however, may be greatly affected by selective chemical and isotopic exchange between the two magmas.

A second source of enclaves could be partly chilled or cumulate material from the margins of the plutons (Bonin, 1991). If the chilled margins were broken up before being completely solid, they would presumably have compositions that closely resemble that of the granite that encloses them. If they represented earlier, higher-temperature magma they would probably be re-incorporated as solid inclusions. In either case, they are likely to have compositions distinct from that of enclaves formed in the first manner.

A third source of enclaves may be from mafic to intermediate magmas that exist in the lower portions of compositionally stratified magma chambers. These magmas may form layers near the base of the chamber and evolve through time by interactions between mafic magmas that were emplaced into and ponded beneath silicic magma. Many studies of silicic volcanic systems support the existence of these intermediate layers, and quenched intermediate enclaves in silicic volcanics are commonly thought to be samples from them (Bacon & Metz, 1984; Grunder, 1994). The compositions of these intermediate layers would be affected not only by selective diffusion and mixing but also by fractional crystallization of the underlying basaltic magma. The evolving composition of the intermediate layer would be particularly dependent on the nature of the cumulus mineral assemblages, the rate of influx of basaltic magma, and the relative volumes of mafic and silicic magmas in the chamber. Fractional crystallization and recharge of the mafic magma could produce intermediate layers with compositions that are distinctly different from hybrid compositions generated by direct mixing of the original mafic and silicic magmas. The compositions of enclaves derived from such intermediate layers may mainly reflect fractionation and hybridization processes that generated the layers rather than exchange processes between enclave and host granite.

Field relations in the Cadillac Mountain intrusive complex provide an exceptional opportunity to understand the processes that have produced magmatic enclaves in a granitic pluton. This shallow-level pluton is tilted so that the base of the intrusion is exposed. A layered gabbro–diorite unit in the lower levels of the granite provides a stratigraphic record of multiple injections of basaltic magma into the silicic magma chamber as well as a record of fractional crystallization and hybridization between basaltic and granitic magmas (Wiebe, 1994; Wiebe *et al.*, 1997). Granitic rocks beneath the gabbro–diorite unit have only very scarce enclaves, whereas, above it, enclaves are common and widely scattered throughout the granite. These relations indicate that the enclaves must almost certainly have come from material

Downloaded from https://academic.oup.com/petrology/article-abstract/38/3/393/1564739
by Trinity University user
on 15 February 2018

that evolved within the chamber, probably from intermediate layers that developed between the basaltic infusions and resident granitic magmas. The purpose of this paper is to present the results of a geochemical study of these enclaves and to relate them to the known compositions of basaltic liquids emplaced into the chamber (preserved as chilled margins on dikes, layers and pillows) and to the fractional crystallization and hybridization history recorded by the gabbro–diorite unit. This plutonic complex provides an intrusive analog to large-volume silicic systems that are thought to have mafic and hybrid underpinnings.

GEOLOGIC SETTING

The Cadillac Mountain intrusive complex (CMIC) occurs on Mount Desert Island, Maine (Fig. 1). It is a part of the Coastal Maine Magmatic Province, which consists of >100 mafic and felsic plutons emplaced over a time span from the Late Silurian to the Early Carboniferous (Hogan & Sinha, 1989). The plutons intrude a variety of metasedimentary and metavolcanic rocks in several fault-bounded, NE–SW-trending terranes featuring different stratigraphies and different structural and metamorphic histories (Williams & Hatcher, 1982). The ages and field relations of many of these plutons suggest that they postdate the main assembly of these lithotectonic terranes (Ludman, 1986). The bimodal character of this province is well established (Chapman, 1962), and there is widespread evidence for commingling between mafic and felsic magmas (Taylor *et al.*, 1980; Stewart *et al.*, 1988; Chapman & Rhodes, 1992; Wiebe, 1993*b*, 1994). Gravity studies (Hodge *et al.*, 1982) indicate that many of the granitic plutons are thin, with gently dipping floors, and probably rest on mafic rocks similar to the interlayered diorite and gabbro that partly surround and dip beneath several of them.

Hornblende from the gabbro–diorite unit in the CMIC gives an Ar–Ar age of about 418 $\pm$ 5 Ma (D. Lux, personal communication, 1993). U–Pb dates of zircons from different phases of the granitic rocks give ages between 419 $\pm$ 2 and 424 $\pm$ 2 Ma (Seaman *et al.*, 1995).

FIELD RELATIONS AND PETROGRAPHY

The CMIC occurs in an irregular, roughly oval area about 14 by 20 km (Fig. 1) (Wiebe, 1994; Wiebe *et al.*, 1997). It consists of three major units: the Cadillac Mountain granite (CMG), a hybrid unit of gabbroic to granitic rocks (G–D), and the Somesville granite (SG). There are, in addition, two smaller units: (1) the sheet-like Southwest Harbor granite, and (2) irregular masses and dikes of the Pretty Marsh granite that cut the G–D unit. The relationships between the major units can be seen more clearly in a schematic east–west cross-section (Fig. 1). The granitic units were emplaced and solidified in the following sequence: Southwest Harbor, Cadillac Mountain, Pretty Marsh and Somesville (Wiebe *et al.*, 1997). Basaltic magmas were emplaced before, during and after these granites, and the G–D unit formed by multiple injections of basaltic magma into the Cadillac Mountain magma chamber (Wiebe, 1994).

Several lines of evidence point to a shallow level of emplacement, perhaps no more than 5–7 km, for the CMIC. The CMG appears to be emplaced into its own eruptive products (Seaman *et al.*, 1995), has common miarolitic cavities in its upper part, and has compositions that plot close to the 500 bar minimum in the system Qtz–Or–Ab–H_2O (Wiebe *et al.*, 1997). Hornblende in the CMG is a ferro-edenite, consistent with low-pressure crystallization (Wiebe *et al.*, 1997). Scarce zones of desilicication in the CMG (Wiebe *et al.*, 1997) may represent reaction between quartz and H_2O-rich vapor at pressures <600 bars (Wiebe, in preparation). Metamorphic mineral assemblages in partially melted pelitic rocks beneath the CMIC commonly include cordierite, andalusite and alkali-feldspar.

Emplacement of the CMIC appears to have been largely controlled by the unconformity between the Ellsworth schist and the gently dipping Bar Harbor Formation. The areal distribution of these country rock units indicates that the unconformity now dips moderately to the southeast, so that the base of the CMIC is exposed along its western and northwestern contacts with the Ellsworth schist (Fig. 1). The Cranberry Island series, a sequence of mainly silicic pyroclastic and lava flow material with subordinate mafic volcanic rocks, lies immediately above the Bar Harbor Formation and south of the CMIC (Fig. 1). Seaman *et al.* (1995) reported an age of 424 $\pm$ 1 Ma for a zircon from these volcanic rocks, indicating that they are contemporaneous with the CMIC. Silicic rocks in the Cranberry Island volcanics have compositions that are most similar to the Southwest Harbor granite (Wiebe *et al.*, 1997). Brief descriptions of the Ellsworth schist and the Bar Harbor Formation have been provided by Gilman *et al.* (1988). To the north, east, and south of the CMIC, dikes and sills of gabbro and diabase occur in the Bar Harbor Formation. The Southwest Harbor granite was emplaced into the lower part of the Bar Harbor Formation and immediately beneath a sill of gabbro. All of these rocks are truncated by an intrusive breccia [termed a 'shatter zone' by Gilman *et al.* (1988)] along the southern margin of the CMG. Steeply dipping masses of gabbro in the Ellsworth schist appear to have been feeders for gabbroic rocks both

Downloaded from https://academic.oup.com/petrology/article-abstract/38/3/393/1564739
by Trinity University user
on 15 February 2018

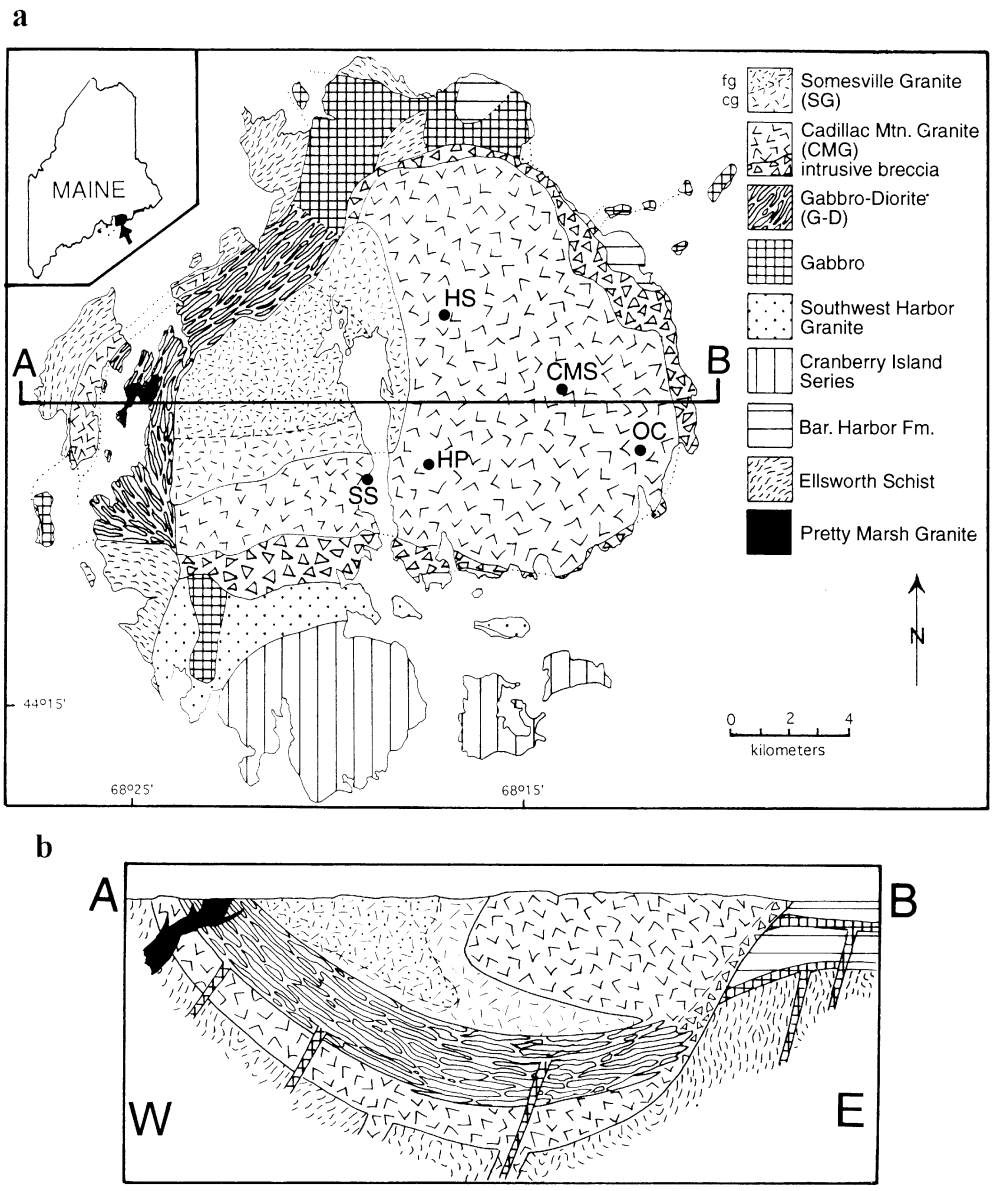

Fig. 1. (a) Geologic map of Mount Desert Island modified from Gilman *et al.* (1988) and Wiebe (1994). Enclave localities: HS, Mount Desert Island High School; CMS, Cadillac Mountain summit; OC, Otter Creek Road; HP, Hadlock Pond; SS, Somes Sound. (b) Schematic cross-section modified from Wiebe (1994). No vertical exaggeration.

within and outside the CMIC; basaltic dikes cut all of the plutonic units, becoming least abundant in the youngest granite (Somesville). Field relations of the granites have been described in more detail by Wiebe *et al.* (1997).

Cadillac Mountain granite

The G–D unit separates the CMG into a lower, apparently sheet-like body and a much larger upper body (Fig. 1). The upper CMG consists of homogeneous, massive, medium- to coarse-grained, hypersolvus granite with a color index (CI) <10. Quartz and mesoperthitic alkali-feldspar are equant and range from 2 to 7 mm in diameter. Larger quartz crystals commonly show resorption channels partly filled with feldspar. Although some alkali-feldspars are unexsolved, most are typically coarsely exsolved, and the relative proportions of plagioclase and alkali-feldspar lamellae suggest that, in different rocks, the original compositions spanned the region between $An_{10}Ab_{85}Or_5$ and $An_2Ab_{30}Or_{68}$ (Wiebe *et al.*, 1997). Hornblende is the dominant mafic mineral;

Downloaded from https://academic.oup.com/petrology/article-abstract/38/3/393/1564739
by Trinity University user
on 15 February 2018

scarce biotite occurs locally. Both minerals are typically interstitial. Ferrohedenbergite occurs sporadically as subhedral to corroded cores in hornblende or as euhedral inclusions in feldspar. Opaque minerals, zircon, and apatite are ubiquitous accessory phases; allanite, titanite, and fluorite are common. The scattered occurrences of fine-grained intermediate plagioclase and local concentrations of small hornblende crystals in the CMG can probably be explained by disaggregation of the more mafic enclaves (see below). Epidote, chlorite, stilpnomelane, carbonate, and sericite occur sparsely as alteration products and, in some rocks, as fillings of primary interstitial cavities.

Granitic rocks within and near the shatter zone are more mafic and varied in mineralogy and texture; some have cumulate textures. These latter rocks contain variable proportions of medium-grained euhedral, sodic alkali-feldspar ($An_5Ab_{70}Or_{25}$) along with minor euhedral to subhedral ferrohedenbergite and, rarely, fayalite (Wiebe *et al.*, 1997). These rocks grade inward from the shatter zone within meters to tens of meters to typical CMG. Fluorite, zircon, and allanite appear to be more abundant in these marginal rocks than in CMG from the interior. These high-temperature silicic cumulates were probably deposited immediately after a major eruptive event which produced the shatter zone and brought hotter and drier magma from a deeper portion of the chamber to higher levels along the chamber wall (Wiebe *et al.*, 1997).

In contrast to the upper CMG, granitic rocks from the lower CMG commonly have two feldspars: normally zoned plagioclase ($An_{30–20}$) and K-rich alkali-feldspar. Although hornblende is the dominant mafic mineral, biotite is common, and both minerals are commonly subhedral. These characteristics are also typical of the granitic portions of the G–D unit.

Gabbro–diorite unit

The gabbro–diorite (G–D) unit of the CMIC consists of interlayered gabbroic, dioritic and granitic rocks with the characteristic field relations of mafic–silicic layered intrusions (MASLI) (Wiebe, 1993*a*). Much of the G–D unit consists of layers of gabbro, typically 2–50 m thick, that occur in macrorhythmic units that grade upward from basally chilled gabbro to coarser-grained gabbroic, dioritic, or granitic rocks. Most of the rocks in this unit are medium grained and have compositions that reflect at least some accumulation of crystals or loss of interstitial liquid owing to compaction and filter-pressing. They can, therefore, be termed cumulates in the sense defined by Irvine (1982) to distinguish them from the chilled parts of the unit that have the compositions of liquids. Loadcast structures are common along the chilled bases of mafic layers, and silicic pipes commonly extend upward from the underlying silicic cumulates [figs 3 and 7 of Wiebe (1994)]. Also common are relatively thin (50–75 cm thick) lensoid to sheet-like masses of gabbro and layers of gabbroic pillows, chilled on all margins, within dioritic to granitic cumulate material [fig. 3 of Wiebe (1994)].

Layers dip moderately (20–50°) to the east in an arcuate pattern roughly conformable with the basinform shape indicated by gravity for both the granite and the gabbro–diorite unit. Silicic pipes are roughly perpendicular to the mafic layers, suggesting that the layers were originally deposited close to horizontal and were subsequently bowed downward as the chamber evolved and solidified. The average exposed thickness of the G–D unit is ~1·5 km.

A detailed section with a stratigraphic thickness of ~50 m illustrates widespread and important features of the G–D unit (Fig. 2). This section includes the bases of three macrorhythmic units, each of which is marked by a prominent chilled gabbro. Subtle chilled horizons also occur within some units, as do horizons with pegmatitic gabbroic patches. Unit F is composite with a lower gabbroic layer that is chilled both on the base (317 m) and on top (331 m) against dioritic cumulate material (Fig. 2). Above that, a few thin lenses of chilled gabbro (lensoid pillows) occur in leucodiorite, which is then capped by another gabbroic layer with a chilled base and a top with prominent pipes which project through the chilled base of G (Fig. 2). Generally, the uppermost part of each unit is the most silicic cumulate material, and silicic pipes, 2–10 cm in diameter, commonly extend upward from the tops of layers into and through the chilled mafic bases of the overlying unit. The top of unit F contains corroded xenocrysts of sodic plagioclase and alkali feldspar. At other locations in the G–D unit, some macrorhythmic units grade up to highly silicic, even granitic, cumulates.

Chilled margins of gabbroic layers typically have basaltic textures with radiating thin laths of strongly zoned plagioclase ($An_{70–30}$). Mafic minerals in chilled margins are dominated by hornblende with subordinate augite, orthopyroxene, Fe–Ti oxides and biotite.

Coarser-grained gabbroic layers are typically massive with randomly arranged, normally zoned plagioclase laths ($An_{70–30}$). Augite and/or hornblende are typically ophitic to subophitic; equant olivine occurs in many layers. Accessory Fe–Ti oxides and apatite are ubiquitous. Plagioclase and augite are the dominant cumulus minerals, and cumulus olivine occurs in some rocks.

Rocks of intermediate composition are dominated by plagioclase and hornblende often with prominent biotite and Fe–Ti oxides, and variable amounts of apatite. Augite and orthopyroxene occur in some rocks, and hornblende commonly contains corroded scraps of augite. Although biotite is typically a minor interstitial phase, it also occurs

Downloaded from https://academic.oup.com/petrology/article-abstract/38/3/393/1564739
by Trinity University user
on 15 February 2018

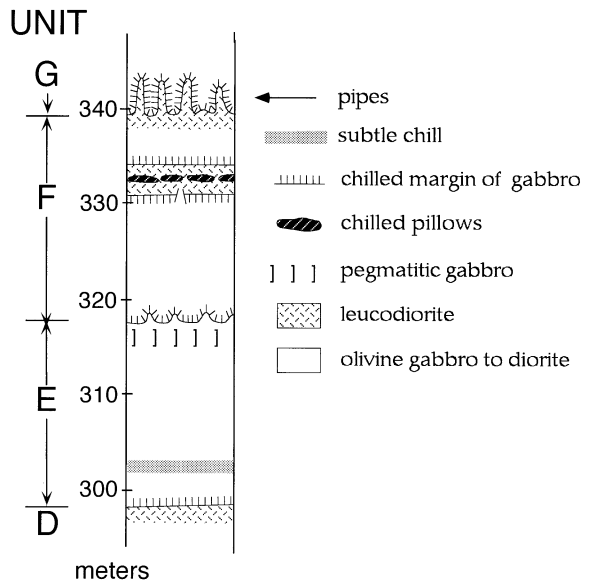

Fig. 2. Stratigraphic section of a characteristic part of the gabbro–diorite unit. Letters refer to the same units as illustrated in fig. 4 of Wiebe (1994).

locally as abundant, large, equant crystals and is the dominant mafic silicate in many diorites. Plagioclase is typically complexly zoned with reverse, oscillatory, and patchy zoning in the interior and normally zoned rims. Interstitial quartz and minor titanite occur in many rocks. Scarce corroded zircons, up to 500 μm in length, occur in most rocks.

In the intermediate rocks there is textural evidence for hybridization between mafic and silicic magmas. In many rocks, plagioclase occurs both as larger corroded, weakly zoned sodic grains and smaller, strongly zoned crystals with calcic cores. In some rocks, intermediate plagioclase contains corroded cores of alkali feldspar, and equant xenocrystic quartz is rimmed by hornblende.

The most silicic portions of the G–D unit occur at the tops of macrorhythmic units or between thin lenses and pillows of chilled basaltic material. These rocks closely resemble the lower Cadillac Mountain granite in terms of grain-size, texture, and mineralogy. Within macrorhythmic units, the upward transition from leucocratic, quartz-poor, plagioclase-rich rock to granite typically occurs over distances of several centimeters.

Magmatic enclaves in the Cadillac Mountain granite

Mafic to silicic magmatic enclaves occur widely but sparsely throughout the CMG, representing <0·1 modal % (Chapman, 1969; Seaman & Ramsay, 1992; Wiebe, 1994). They range in size from <1 cm to >1 m in diameter. In the outer portions of the upper CMG, most magmatic enclaves are strongly flattened, and their attitudes appear to define a basinform shape (Chapman, 1969; Gilman *et al.*, 1988) that conforms to the shape of the chamber floor suggested by gravity studies. Magmatic enclaves are much less abundant in the lower CMG and rare to absent in granite that lies within and immediately adjacent to the shatter zone.

The textures and mineralogy of the enclaves are variable. Although these variations appear to be gradational, the enclaves can be divided reasonably well into three main types: (1) a relatively mafic, fine- to medium-grained group (mainly diorites) dominated by hornblende and intermediate plagioclase; (2) a more leucocratic, finer-grained group (mainly monzodiorites) with Fe-rich augite and sodic plagioclase, ternary feldspar, or alkali-feldspar; (3) a fine-grained silicic group (granite) dominated by alkali-feldspar, quartz and interstitial hornblende. (We use the term 'mafic' in reference to type 1 enclaves, but note that this term is used only in the relative and not the strict sense.) The first two types range from a few millimeters to ~30 cm in diameter and generally lack chilled margins. They are commonly found in the same outcrop. The third type is typically ~20 cm to 1 m in diameter and commonly has chilled crenulate margins against the host granite. All but one enclave of this type was sampled in a restricted area near the summit of Cadillac Mountain. Nearly all of the enclaves have been affected to some extent by subsolidus alteration that produced some of the following phases: stilpnomelane, epidote, chlorite, fluorite, calcite, and sericite.

Seaman & Ramsey (1992) reported two unusual features related to the margins of some enclaves: the presence of slightly coarser mafic 'satellite' clots in granite near an enclave, and the occurrence of a thin rim of unusually felsic material around an enclave. We only very rarely encountered enclaves that displayed these characteristics, and we were unable to sample any of them.

Most common and widespread are relatively mafic enclaves (type 1) with subequant to irregular shapes and a size range of 0·5–2 cm in diameter; some are rarely as large as 10 cm. Many are sufficiently small that they appear in outcrop to be mafic interstitial areas between the coarse-grained feldspar and quartz. They generally have diabasic to equigranular textures and are typically dominated by subhedral, tabular plagioclase and interstitial hornblende with subordinate opaque minerals and apatite; in many, corroded patches of augite commonly occur within hornblende. CI is typically 25–35. Interstitial quartz and alkali-feldspar vary from 5 to 15 vol. %. Interstitial biotite is common in rocks with low amounts of alkali-feldspar and is essentially absent in enclaves with substantial alkali-feldspar. Plagioclase ranges in size from 0·2 to 4 mm and in composition from An_{45} to An_{10}. Crystals with more calcic cores commonly show complex

Downloaded from https://academic.oup.com/petrology/article-abstract/38/3/393/1564739
by Trinity University user
on 15 February 2018

zoning with coarse reversals following episodes of resorption and rounding. Large sodic patches within some plagioclase cores connect to sodic rims and record late-stage resorption of the plagioclase (Vance, 1965). As the abundance of alkali-feldspar increases, it begins to occur as prominent rims of mesoperthite around plagioclase cores that may be either euhedral or strongly corroded. Individual enclaves commonly contain feldspar crystals with very different compositions and zoning characteristics. Euhedral to corroded zircon occurs as an accessory phase in most type 1 enclaves; titanite, allanite and fluorite occur in some as scarce interstitial grains. These enclaves lack any evidence of quenched margins, and there is no systematic zoning from center to rim in the grain-size, abundances of minerals, or the occurrence of relict augite.

More leucocratic (CI = 10–20), fine-grained, intermediate enclaves (type 2) are equant to lensoid in shape and range from ~2 to 30 cm in diameter. Some are composite with smaller, more mafic inclusions. They are characterized by feldspar and clinopyroxene, mostly ranging in size from 0·1 to 0·3 mm. Clinopyroxene is typically subhedral to euhedral and evenly disseminated. Feldspar varies from a sodic plagioclase or ternary feldspar to mesoperthite. Scarce phenocrysts of feldspar, some with sodic plagioclase cores, and clinopyroxene are up to 2 mm in diameter. Feldspar phenocrysts commonly contain small inclusions of clinopyroxene, often in a zonal arrangement. Up to ~10% interstitial quartz may be present. Generally, hornblende occurs only locally in small patches, and biotite is absent. Minute grains of Fe–Ti oxides and highly acicular apatite are widely disseminated. Corroded zircons up to a few hundred microns occur very sparsely. Corroded xenocrysts of quartz are common and typically rimmed by small clinopyroxene crystals. Larger feldspar crystals are also present in some enclaves. Although these enclaves have textures that are consistent with quenched liquids and their margins are molded around adjacent crystals in the CMG, most lack finer-grained margins. Hornblende has partly replaced clinopyroxene in many type 2 enclaves and one 3-cm enclave has a hornblende-bearing margin ~2 mm thick. Another enclave displays a gradual transition from an area with clinopyroxene to one with hornblende; this transition is truncated by the enclave margin. These relations suggest that there was very little movement of volatiles from the host granite into the enclaves. Some enclaves of this type contain a few equant areas, 2–3 mm in diameter, that consist of quartz surrounded by inward-projecting euhedral feldspar crystals. These structures may be amygdules and, hence, record vesiculation of the enclave magma. Similar features have been interpreted as inclusions of granitic magma [fig. 9 of Bussell (1991)].

The most leucocratic (CI = 2–10) enclaves (type 3) appear to be largely restricted to an area near the summit of Cadillac Mountain. They consist of irregularly shaped, fine-grained enclaves of variably porphyritic silicic material with chilled and crenulate margins and may be up to a few meters in diameter. In some areas, the arrangements of these 'blobby', silicic enclaves define irregular curvilinear zones (~1 m wide and several meters long) suggesting they formed from the disruption of silicic dikes passing through partially solidified granite. They appear to be randomly distributed in other areas. Their unusual occurrence and compositions led Wiebe & Adams (1995) to interpret them as magmas from the upper part of the CMG magma chamber that were trapped as quenched blobs as they passed upward through the semi-crystalline roof of the chamber during an eruption.

These silicic enclaves have textures that are dominated by equant crystals and granophyric intergrowths of mesoperthitic alkali-feldspar and quartz typically ranging in size from 0·1 to 0·5 mm. The mafic minerals consist mainly of interstitial hornblende and biotite in varying proportions along with scarce small equant Fe–Ti oxides and minute crystals of acicular apatite. Scarce, small clinopyroxene grains occur within some feldspar crystals. Rounded xenocrysts of quartz and feldspar grains are common and resemble crystals in the host CMG. Rarely, these enclaves are composite, with incompletely mixed inclusions consisting of very fine-grained clinopyroxene and alkali-feldspar (type 2). Some of this included material is strongly quenched with skeletal, radiating clusters of clinopyroxene in a very fine-grained matrix of mesoperthite.

GEOCHEMISTRY

Major- and trace-element analyses have been obtained for >400 rocks of the CMIC using X-ray fluorescence (XRF), inductively coupled plasma (ICP), and instrumental neutron activation analysis (INAA). Major elements and some trace elements (Rb, Sr, Ni, Nb, Ga, Cu, Zn, U, and Th) were determined by XRF using a Phillips PW2400 spectrometer with an Rh tube. For major-element analysis, 3·6 g of $Li_2B_4O_7$ were mixed with 0·4 g of rock powder and fused into a homogeneous glass disk. Working curves were determined by analyzing 51 geochemical rock standards, data for each having been compiled most recently by Govindaraju (1989). Trace elements were analyzed using a pressed powder briquette consisting of 1·4 g of microcrystalline cellulose and 7·0 g of sample. Other trace elements (Ba, Y, Zr, Cr, Be, Co, Sc, Ce, and Yb) were determined using a Thermo Jarrel Ash Corp. inductively coupled atomic plasma spectrometer. Sample (0·2 g) and

Downloaded from https://academic.oup.com/petrology/article-abstract/38/3/393/1564739
by Trinity University user
on 15 February 2018

$LiBO_2$ (0·7 g) were mixed, fused, and dissolved in a 6% HNO_3 solution containing 2 p.p.m. Cd as an internal standard. Sixteen rock standards were prepared in the same manner and used to construct working curves. Repetitive analyses of standards suggest that errors for SiO_2 and MgO are $\pm 1\%$ (relative to the amount present), and relative errors for other major elements are $\pm 2\%$, except Na_2O, which is $\pm 5\%$. Analyses of standards suggest that the accuracy of most trace element analyses is largely between ± 5 and $\pm 10\%$. REE analyses were done at the Oregon State University Radiation Center; estimated error is between ± 3 and $\pm 7\%$, except for Nd, where error may be as high as $\pm 12\%$ (relative to amount present).

Representative analyses of all units have been listed by Wiebe (1994); all available analyses of the CMG have been listed by Wiebe *et al.* (1997). Here we present compositional data for basaltic dikes, mafic to silicic rocks of the G–D unit, and magmatic enclaves in the CMG.

Chilled mafic rocks

The chilled margins of layers and pillows in the G–D unit and basaltic dikes that cut the CMIC have very similar compositions and compositional ranges for all major and trace elements (Table 1, Fig. 3). Both groups are subalkaline and straddle the boundaries between tholeiites and calc-alkaline basalts on most discriminant diagrams, and range from olivine to quartz normative. Their compositions form relatively tight clusters on Harker diagrams (Figs 4 and 5). Rare earth element (REE) concentrations in these rocks show a modest enrichment in light REE (LREE) with chondrite-normalized La/Lu mainly between 1·4 and 3·4 and La ranging between 17 and 72 times chondrites (Table 1, Fig. 6a). The rocks either lack an Eu anomaly or have small negative or positive anomalies. The compositional range and trends of the chilled liquids are generally consistent with variable fractional crystallization of plagioclase, olivine and augite at depth, before emplacement of the basaltic magmas into the CMIC. However, scatter in alkalis and wide ranges in some incompatible element ratios suggest either some selective contamination by crustal material or perhaps *in situ* crystallization processes [see Langmuir (1989)].

Medium-grained rocks (cumulates) from the gabbro–diorite unit

The compositions of medium-grained rocks from layers in the G–D unit range from ~44 to 75 wt % SiO_2 (Table 2, Figs 4 and 5). MgO varies from <1 to >16 wt %, but only a few samples have between 4 and 7 wt % MgO (Fig. 4). The rocks with lowest SiO_2 have compositions that are consistent with their being cumulates from liquids comparable in composition with the chilled margins of gabbroic layers and basaltic dikes, whereas rocks with the highest SiO_2 closely approximate the average compositions of the CMG. The compositions of rocks with intermediate SiO_2 cannot be solely explained by bulk mixing between basaltic and granitic compositions but must also have been affected by crystal accumulation and loss of interstitial liquid owing to compaction and formation of pipes. Accumulation of plagioclase and mafic silicates is supported by relatively high concentrations of MgO, CaO, and Sr (Figs 4 and 5). The wide scatter of alkalis may reflect variable alkali exchange between commingling mafic and silicic magma.

These rocks show a wide range in REE concentrations (Table 2, Fig. 6b). The most mafic cumulates have nearly flat REE patterns, weak positive Eu anomalies, and abundances <10 times chondrites; the most silicic layers have LREE-enriched patterns, moderate to strong negative Eu anomalies, and La up to 120 times chondrites. The two rocks with >70% SiO_2 have positive Ce anomalies. The most mafic cumulates have REE abundances and patterns that are consistent with accumulation of plagioclase and mafic silicates from parental liquids with compositions similar to the chilled basaltic layers and dikes (Fig. 6a,b).

Figure 7 shows the compositional variation that occurs in a stratigraphic section, part of which (units E and F) is illustrated in Fig. 2. Each new injection of basaltic magma is marked by a chilled basaltic layer with a lower concentration of K, Rb and Ba than the underlying layer. Immediately above the chilled base, the mafic rocks take on a cumulate character and generally have still lower concentrations of these incompatible elements. On the basis of petrographic evidence, the overall upward increase in these elements within each macrorhythmic unit appears to reflect both fractional crystallization of basaltic magma and hybridization with overlying CMG magma.

Magmatic enclaves in the CMG

Twenty-six different enclaves were analyzed, and compositions were obtained for the core and rim of one of these (Table 3). The ranges in wt % SiO_2 for the enclave types are: type 1 ('mafic'), 55–61; type 2 ('intermediate'), 62–68; and type 3 ('silicic'), 70–78. There is essentially no overlap between the compositions of the enclaves and the chilled mafic rocks (Figs 4 and 5): only two chilled mafic rocks have >53% SiO_2. Enclave compositions produce relatively coherent trends for most elements plotted against SiO_2, but do show considerable scatter in the concentrations of alkalis (Figs 4 and 5). The silicic enclaves produce a distinctly different and steeper trend for Sr vs SiO_2 than types 1 and 2 (Fig. 5). Relative to

Downloaded from https://academic.oup.com/petrology/article-abstract/38/3/393/1564739
by Trinity University user
on 15 February 2018

Table 1: Chemical analyses of basaltic dikes and chilled margins of gabbroic layers in the gabbro–diorite unit; for elements determined by more than one method, results by the most accurate method are reported

	Dikes							
	116B	6C	8	32C	13	EMS-4C	45A	60
Major elements (wt %)								
SiO_2	47·26	48·39	48·42	48·85	50·45	50·57	51·83	53·30
TiO_2	1·71	1·56	1·66	1·35	1·46	1·02	1·75	1·94
Al_2O_3	16·22	15·58	16·01	16·41	16·01	15·32	15·72	15·12
Fe_2O_3	3·62	1·68	2·75	1·99	1·90	9·22	2·58	2·19
FeO	7·51	8·40	7·67	6·98	7·28	n.a.	7·36	8·31
MnO	0·18	0·19	0·18	0·18	0·16	0·15	0·17	0·18
MgO	7·64	8·75	8·05	8·35	6·69	8·20	6·09	4·26
CaO	10·52	9·40	10·99	10·57	10·05	9·14	8·24	7·39
Na_2O	2·93	2·98	2·75	2·38	3·60	3·13	3·21	3·08
K_2O	0·21	0·87	0·26	0·66	0·68	0·52	1·10	1·62
P_2O_5	0·16	0·22	0·20	0·13	0·21	0·15	0·33	0·35
LOI	2·62	2·34	2·53	2·25	2·59	1·92	1·72	1·43
Total	100·58	10·36	101·47	100·10	101·08	99·34	100·10	99·17
Trace elements (p.p.m.)								
Ni	122	162	105	106	96	135	88	33
Sc	37	33	39	36	33	32	27	26
Cr	214	361	280	246	199	382	175	63
Co	12	44	43	43	36	40	44	46
V	243	224	245	212	218	195	197	236
Rb	12	46	15	34	24	17	40	52
Sr	260	220	265	236	238	276	253	333
Ba	55	113	51	85	118	112	149	291
Y	33	33	34	34	37	47	42	38
Zr	124	122	140	131	181	117	202	199
Nb	4	4	3	3	5	7	7	9
Ga	19	17	19	17	18	18	20	19
Be	0·6	1·1	1·2	1·2	1·3	1·5	1·6	1·7
La	n.a.	n.a.	6·95	n.a.	12	n.a.	n.a.	21·3
Ce	24·0	24·2	18·0	22·7	27·6	35·0	48·4	45·4
Nd	n.a.	n.a.	12·6	n.a.	16·8	n.a.	n.a.	22·9
Sm	n.a.	n.a.	4·24	n.a.	5·15	n.a.	n.a.	6·19
Eu	n.a.	n.a.	1·46	n.a.	1·51	n.a.	n.a.	1·77
Tb	n.a.	n.a.	0·85	n.a.	0·88	n.a.	n.a.	1·06
Yb	2·60	2·78	2·92	3·20	3·21	3·80	3·62	3·36
Lu	n.a.	n.a.	0·41	n.a.	0·45	n.a.	n.a.	0·47
Cu	63	54	75	56	52	26	45	25
Zn	65	134	91	76	82	78	90	107
U	n.d.	1·0	n.d.	1·8	1·1	n.d.	n.d.	0·9
Th	n.d.	n.d.	n.d.	n.d.	n.d.	n.d.	n.d.	2·0
Hf	n.a.	n.a.	3·1	n.a.	4·0	n.a.	n.a.	4·5
Ta	n.a.	n.a.	0·3	n.a.	0·4	n.a.	n.a.	0·8

Downloaded from https://academic.oup.com/petrology/article-abstract/38/3/393/1564739
by Trinity University user
on 15 February 2018

Table 1: continued

	Chilled margins								
	6A	EMS-2B	MS-15	EMS-3A	EMS-5D	126A	44A	65A	38A
Major elements (wt %)									
SiO_2	46·63	46·70	47·31	47·60	47·75	48·00	48·04	48·18	48·31
TiO_2	1·12	1·85	1·25	1·66	1·94	1·89	1·89	1·24	1·25
Al_2O_3	17·80	16·16	17·28	15·98	16·52	16·08	16·03	17·88	16·33
Fe_2O_3	1·33	12·07	9·39	11·37	12·31	2·53	2·48	2·31	2·57
FeO	8·50	n.a.	n.a.	n.a.	n.a.	8·44	8·29	7·06	7·02
MnO	0·15	0·18	0·14	0·17	0·18	0·18	0·19	0·16	0·20
MgO	8·47	7·09	8·54	6·96	7·45	6·53	7·12	9·05	7·45
CaO	9·44	10·68	11·21	10·51	9·98	9·19	9·96	11·18	10·88
Na_2O	2·91	3·13	2·77	3·38	3·32	3·39	2·88	2·56	2·68
K_2O	0·59	0·81	0·27	0·72	0·62	0·79	0·79	0·15	0·60
P_2O_5	0·13	0·32	0·19	0·28	0·34	0·34	0·35	0·09	0·13
LOI	3·80	1·57	0·38	0·83	0·65	3·48	1·62	0·97	2·13
Total	100·87	100·56	98·73	99·46	101·06	100·84	99·64	100·83	99·55
Trace elements (p.p.m.)									
Ni	156	57	118	53	86	51	84	118	112
Sc	33	37	36	38	34	30	32	38	36
Cr	250	170	542	250	156	116	153	241	212
Co	44	41	46	39	43	0	38	45	42
V	198	269	205	270	257	235	257	228	212
Rb	28	17	7	11	17	28	26	6	23
Sr	213	397	268	385	329	350	321	224	247
Ba	91	132	62	182	125	131	168	37	112
Y	32	31	20	28	37	37	37	32	31
Zr	101	111	87	103	159	164	162	85	108
Nb	4	5	4	4	6	7	6	2	2
Ga	19	18	17	18	19	19	19	17	17
Be	1·7	1·4	0·9	1·5	1·5	0·8	1·0	1·0	1·1
La	8·45	n.a.	6	n.a.	n.a.	n.a.	n.a.	n.a.	5·37
Ce	20·1	21·0	15·0	30·0	37·0	41·3	30·2	12·8	13·8
Nd	12·4	n.a.	9	n.a.	n.a.	n.a.	n.a.	n.a.	11
Sm	3·61	n.a.	2·60	n.a.	n.a.	n.a.	n.a.	n.a.	3·47
Eu	1·10	n.a.	1·10	n.a.	n.a.	n.a.	n.a.	n.a.	1·19
Tb	0·68	n.a.	0·60	n.a.	n.a.	n.a.	n.a.	n.a.	0·72
Yb	2·84	2·30	1·90	2·00	3·00	3·10	3·10	2·90	2·65
Lu	0·39	n.a.	0·30	n.a.	n.a.	n.a.	n.a.	n.a.	0·38
Cu	60	63	62	55	52	27	55	64	72
Zn	91	82	62	84	93	92	97	67	85
U	n.d.	1·2	n.d.	1·3	n.d.	0·6	n.d.	1·2	n.d.
Th	n.d.	n.d.	n.d.	n.d.	n.d.	n.d.	n.d.	n.d.	n.d.
Hf	2·5	n.a.	0·8	n.a.	n.a.	n.a.	n.a.	n.a.	2·6
Ta	0·3	n.a.	0·5	n.a.	n.a.	n.a.	n.a.	n.a.	0·1

Downloaded from https://academic.oup.com/petrology/article-abstract/38/3/393/1564739
by Trinity University user
on 15 February 2018

Table 1: continued

	Chilled margins												
	117A	42B	EMS-4D	43A	110A	41A	MS-7	MS-10	117B	MS-2	70	O-2	32A
Major elements (wt %)													
SiO_2	48·41	48·57	49·39	49·42	49·58	49·67	49·80	49·99	50·46	50·52	50·69	51·12	56·04
TiO_2	1·84	1·70	1·62	2·48	1·31	1·33	1·89	1·86	2·22	1·07	1·94	1·95	1·79
Al_2O_3	13·82	15·79	15·94	14·86	17·12	15·39	15·90	17·08	15·26	16·84	15·24	15·87	14·96
Fe_2O_3	2·47	2·05	11·10	3·77	2·18	2·20	10·10	11·18	2·59	8·85	2·88	1·45	2·07
FeO	9·50	8·29	n.a.	9·11	6·49	7·46	n.a.	n.a.	8·83	n.a.	7·84	8·53	6·43
MnO	0·20	0·22	0·17	0·22	0·15	0·16	0·17	0·17	0·20	0·14	0·18	0·17	0·15
MgO	9·28	6·75	6·76	4·46	7·34	6·78	6·48	6·80	5·68	7·09	5·68	5·98	3·81
CaO	8·51	8·58	10·16	7·89	10·78	10·04	9·50	9·60	8·37	9·80	8·42	8·72	6·74
Na_2O	3·13	3·10	3·55	3·82	2·99	3·16	3·11	3·08	3·68	3·05	3·40	3·38	3·97
K_2O	0·62	0·83	0·92	1·30	0·30	0·82	0·94	0·85	1·04	0·89	1·32	1·10	1·64
P_2O_5	0·30	0·23	0·27	0·48	0·12	0·18	0·32	0·27	0·38	0·15	0·36	0·34	0·28
LOI	1·24	2·98	1·01	1·57	1·71	2·56	2·00	0·68	1·63	0·40	1·56	1·64	3·24
Total	99·32	99·09	100·89	99·38	100·07	99·75	100·21	101·56	100·34	98·80	99·51	100·25	101·12
Trace elements (p.p.m.)													
Ni	191	122	50	35	122	90	70	78	54	70	81	58	23
Sc	34	31	35	30	40	32	30	34	32	33	28	29	24
Cr	518	184	157	67	207	259	151	163	121	237	124	150	68
Co	0	50	40	59	27	41	37	43	0	42	45	33	0
V	240	218	254	263	230	219	247	261	254	173	210	244	193
Rb	18	38	23	41	12	25	18	20	29	28	70	35	69
Sr	247	260	374	309	232	276	274	260	283	230	244	310	280
Ba	165	164	271	609	44	211	164	151	189	144	143	283	343
Y	42	35	28	53	35	37	32	30	49	25	45	39	42
Zr	172	143	109	267	105	109	193	146	267	128	197	193	211
Nb	5	6	4	9	2	5	n.a.	7	9	5	8	8	9
Ga	19	18	18	22	17	18	n.a.	18	21	17	19	20	19
Be	0·6	1·4	1·5	1·8	0·9	1·4	0·9	1·4	0·3	1·1	1·5	1·2	1·4
La	n.a.	11·5	n.a.	22·8	6·59	14·1	14	13	17·8	11	n.a.	n.a.	n.a.
Ce	38·4	26·3	28·0	49·0	14·6	31·3	35·0	29·0	40·2	24·0	49·6	41·0	58·1
Nd	n.a.	15·9	n.a.	29·4	11·7	18·2	18·0	15	26	12	n.a.	n.a.	n.a.
Sm	n.a.	4·64	n.a.	8·43	3·77	4·83	4·80	4·20	7·34	3·20	n.a.	n.a.	n.a.
Eu	n.a.	1·48	n.a.	2·54	1·27	1·47	1·70	1·80	2·27	1·50	n.a.	n.a.	n.a.
Tb	n.a.	0·84	n.a.	1·33	0·82	0·91	0·80	0·90	1·23	0·30	n.a.	n.a.	n.a.
Yb	3·60	3·04	1·90	4·73	3·07	3·21	3·10	2·50	4·28	2·20	3·70	3·20	3·50
Lu	n.a.	0·43	n.a.	0·66	0·43	0·44	0·50	0·40	0·60	0·40	n.a.	n.a.	n.a.
Cu	42	49	61	40	85	45	n.a.	39	36	44	40	39	27
Zn	102	131	81	139	63	82	n.a.	83	111	65	95	88	79
U	n.d.	1·9	n.d.	n.d.	n.d.	n.d.	0·6	0·5	1·6	n.d.	3·1	n.d.	2·1
Th	n.d.	n.d.	0·7	n.d.	n.d.	n.d.	1·8	1·3	n.d.	4·3	n.d.	n.d.	3·6
Hf	n.a.	3·4	n.a.	5·8	2·6	3·3	4·7	3·7	5·9	3·3	n.a.	n.a.	n.a.
Ta	n.a.	0·5	n.a.	0·7	n.d.	0·4	0·5	0·5	0·7	0·5	n.a.	n.a.	n.a.

n.a., not analyzed; n.d., not detected.

Downloaded from https://academic.oup.com/petrology/article-abstract/38/3/393/1564739
by Trinity University user
on 15 February 2018

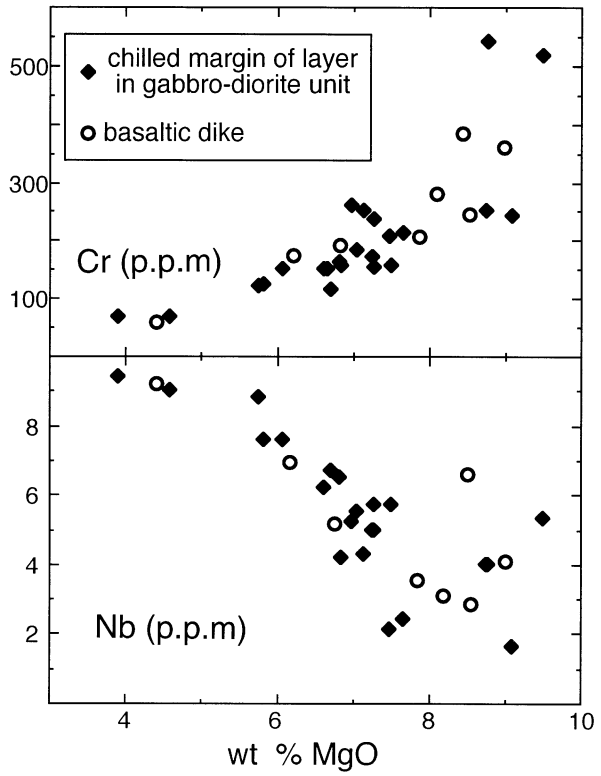

Fig. 3. MgO vs Cr and Nb for basaltic dikes and chilled margins of layers within the gabbro–diorite unit.

most cumulates of the G–D unit, most enclaves are greatly enriched in Y, Yb, Ce, Nb, Ga, and Be; the concentrations of these elements are greatest in enclaves with the lowest SiO_2 and decrease strongly as SiO_2 increases (Fig. 5). Relative to most G–D cumulates, the enclaves are depleted in MgO, CaO and Sr. Compared with chilled basalts, the enclaves with the lowest SiO_2 are enriched in Ga, Zn, Na, K, Rb, Ba, Zr, Y, Hf, Ta, Ce, Sm, Yb, Be, Nb, U, and Th, and are strongly depleted in most elements that are compatible with respect to plagioclase, olivine, pyroxene and titanomagnetite (Ni, Cr, Mg, Cu, V, Co, Sr, Ca, Sc, and Ti) (Figs 5 and 8).

Most enclaves have REE patterns with flat LREEs and only slightly lower heavy REE (HREE) with strong negative Eu anomalies; La varies between 90 and 210 times chondrites (Table 3, Fig. 6c). The two analyzed enclaves with >70 wt % SiO_2 have REE concentrations and patterns resembling those for the CMG (Wiebe *et al.*, 1997). Although they have similar La, Ce, and Eu contents compared with the other enclaves, concentrations of the other REEs are notably lower in these two rocks.

The type 1 enclaves have REE abundances and patterns that are consistent with liquids that could have evolved by fractional crystallization of plagioclase and mafic silicates from liquids comparable to chilled mafic rocks in the G–D unit (Fig. 6). For example, the positive Eu anomalies shown by many of the cumulate rocks are complementary to the negative Eu anomalies of the enclaves.

For some elements, there appear to be geochemical variations that are related to enclave location. For example, there are two compositional groups of enclaves defined by different concentrations of Be vs SiO_2 (Fig. 9). Samples from the high-Be group (all groups but the Otter Cliffs Road samples), which also tend to be enriched in REEs, Nb, and Ga, occur within a large interior area of the CMG, whereas samples from the low-Be group (Otter Cliffs Road samples) occur in the outer portion of the CMG within 2 km of the shatter zone (Fig. 1). Enclaves taken from a single outcrop commonly show distinctive chemical characteristics compared with enclaves taken from other sampled outcrops. For example, three enclaves from Hadlock Pond have SiO_2 ranging from ~57 to 69 wt % and consistently low K_2O and K/Rb compared with most other enclaves (Fig. 9). In contrast, two enclaves from Somes Sound have similar SiO_2 contents (~65 wt %), but very different alkali contents (~0·5 wt % vs 5 wt % K_2O; ~80 vs ~230 K/Rb) (Fig. 9).

DISCUSSION

Origin of compositional variation in the magmatic enclaves

The mafic and intermediate enclaves (types 1 and 2) appear to vary continuously in SiO_2 from ~55 to 70 wt %. Except for the alkalis and several incompatible trace elements, the compositions produce tight linear to slightly curved trends on Harker diagrams from the most mafic enclave to the average composition of the CMG (Figs 4 and 5). Although this variation provides a strong argument for a genetic link between the enclaves, there are several reasons why these trends to high SiO_2 cannot be due largely to fractional crystallization: (1) there is abundant petrographic evidence for incomplete mixing and hybridization in many enclaves, especially in those with intermediate compositions; (2) several trace elements (e.g. Be, Nb, Zn, Ga) which are incompatible with the bulk crystallizing mineral assemblage decrease strongly with increasing SiO_2; (3) the more mafic enclaves contain relatively abundant hydrous phases (hornblende and biotite), whereas the more evolved intermediate enclaves are relatively dry with mesoperthite and clinopyroxene. For all of these reasons, it is much more likely that the variation from low to high SiO_2 is largely related to hybridization between a mafic liquid and resident silicic magma. On the basis of their chemical compositions and

Downloaded from https://academic.oup.com/petrology/article-abstract/38/3/393/1564739
by Trinity University user
on 15 February 2018

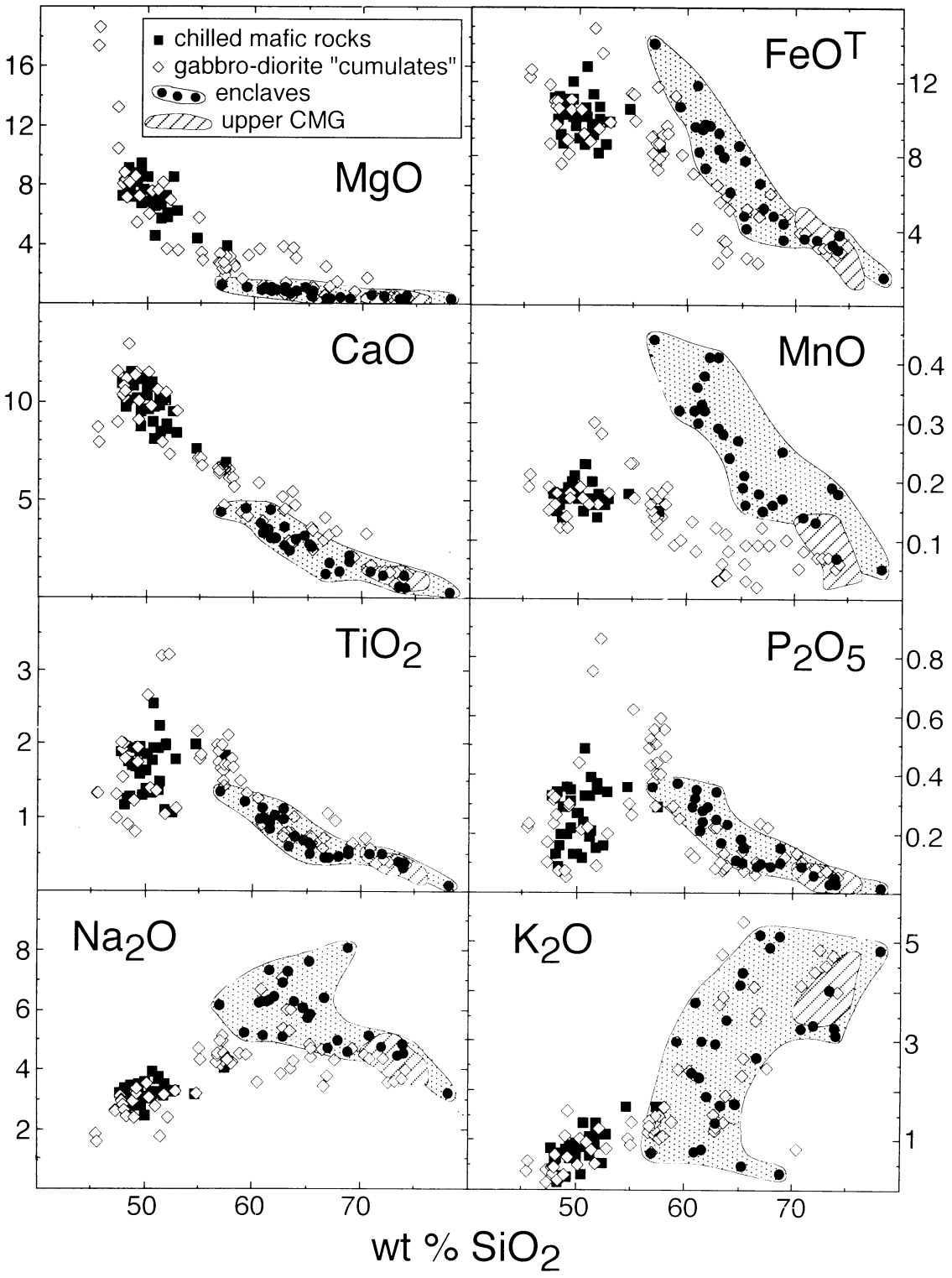

Fig. 4. Plots of selected major elements vs SiO_2 for chilled mafic rocks (dikes and chilled margins in G–D unit), medium-grained 'cumulates' from the G–D unit, and enclaves from the Cadillac Mountain granite. The enclosed dashed field shows the compositional range of the upper Cadillac Mountain granite; a table of these data has been given by Wiebe *et al.* (1997).

Downloaded from https://academic.oup.com/petrology/article-abstract/38/3/393/1564739
by Trinity University user
on 15 February 2018

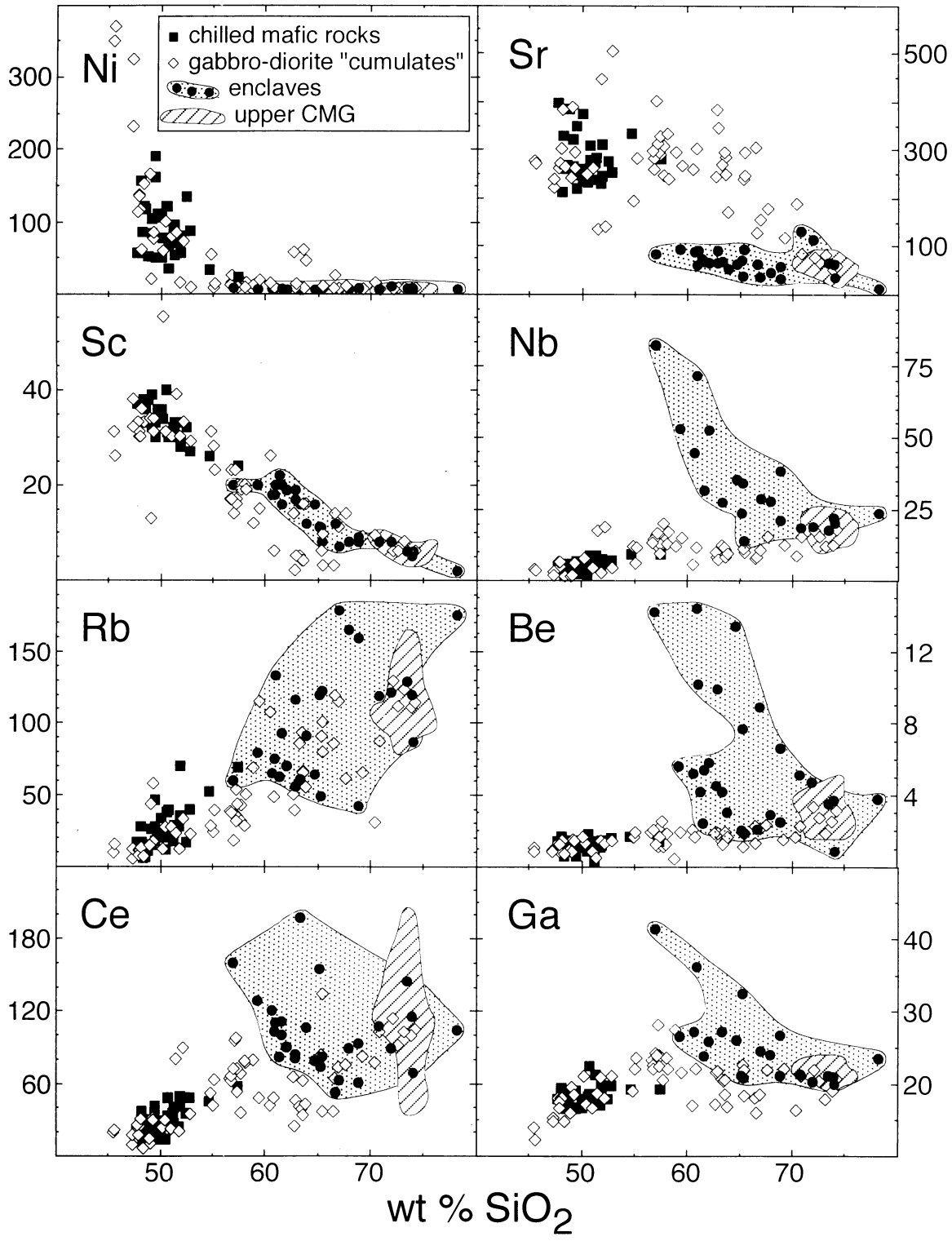

Fig. 5. Plots of selected trace elements vs SiO_2 for the same rocks as plotted in Fig. 4.

Downloaded from https://academic.oup.com/petrology/article-abstract/38/3/393/1564739
by Trinity University user
on 15 February 2018

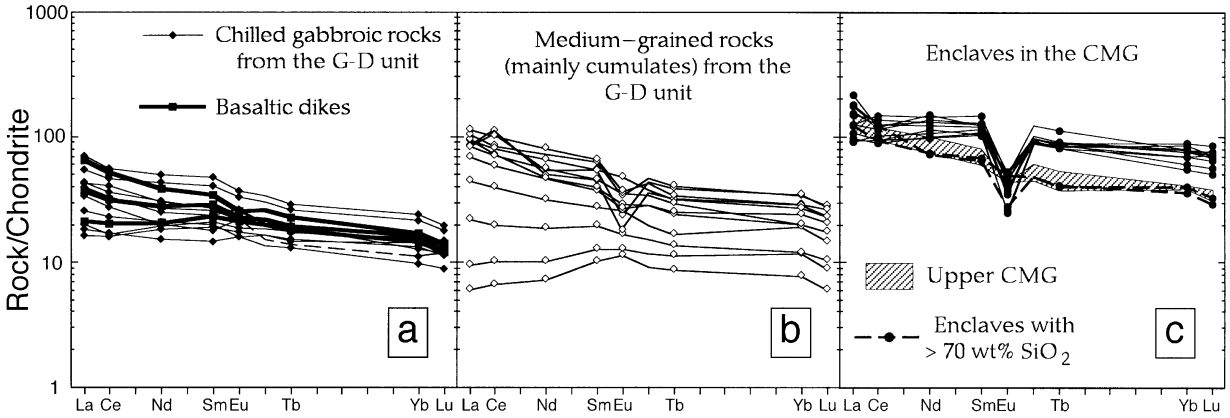

Fig. 6. Plots of REEs normalized to chondrites. (a) All chilled mafic rocks (dikes and layers in the gabbro–diorite unit). (b) Cumulates from the gabbro–diorite unit. (c) Enclaves in the CMG.

textures, the most mafic enclaves are likely to represent the least contaminated magma that mixed with silicic magma in the CMG magma chamber.

The trend from hydrous mineral assemblages in mafic enclaves to relatively anhydrous mineral assemblages in more silicic enclaves is also seen in gradations from mafic to felsic rocks in macrorhythmic units of the Pleasant Bay intrusion (Wiebe, 1993*b*). This trend can be best explained by exchange of H_2O between stably stratified mafic and silicic magmas, enhanced by stable growth of hornblende and biotite in the mafic magma (Coulon *et al.*, 1984; Wiebe, 1993*b*). Growth of these hydrous minerals is commonly noted along the margins of chilled mafic pillows in granite (Wiebe, 1973) and has been observed in some experiments with coexisting mafic and silicic magmas (Johnston & Wyllie, 1988; Van der Laan & Wyllie, 1993).

The wide scatter in the concentrations and ratios of the alkalis is understandable in the context of the hybridization between mafic and felsic magmas that produced the enclave compositions. Exchange of alkalis has long been noted at the boundaries of chilled mafic pillows in granite (Wiebe, 1973) and in experiments with coexisting mafic and silicic magmas (Watson & Jurewicz, 1984). On a larger scale in the nearby Gouldsboro granite, Wiebe & Adams (1995) have suggested that rapid exchange of alkalis between commingling mafic and normal granitic magmas at the base of the chamber led to the formation of a layer of low-K (and low-Rb) trondhjemitic magma beneath high-K granitic magma.

The concentrations of several incompatible trace elements (e.g. Be, Ce, Ga; see also Fig. 9) vary widely in enclaves of comparable size from different localities. As the concentrations of these elements in the host granite are essentially the same at all locations, these relations suggest that the trace element character of the enclaves is inherited from compositionally distinct mafic end-members (see below).

For most elements, the silicic enclaves appear to extend the trends of the mafic and intermediate enclaves to 78% SiO_2. For some elements, however, these silicic enclaves produce trends that are distinct from the other enclaves. On most Harker diagrams they produce smooth trends that pass through the typical composition of the CMG and show decreasing Na_2O and Sr, and increasing Nb as SiO_2 increases (Figs 4 and 5). These variations can be largely explained by fractional crystallization of feldspar.

Does hybridization shown by enclaves reflect local or remote processes?

Many recent workers have focused on the importance of mechanical and chemical exchange between enclaves and the immediately surrounding host granite (e.g. Bedard, 1990; Bussy, 1991; Debon, 1991; Holden *et al.*, 1991; Orsini *et al.*, 1991; Blundy & Sparks, 1992; Seaman & Ramsey, 1992). These studies emphasize possible re-equilibration of enclave with host granite so that crystallization of phases in the enclave (hornblende, apatite, allanite, zircon, etc.) controls the concentration of many elements within the enclave. Growth of these minerals is thought to influence the diffusion of elements that are compatible in these phases (e.g. Y in hornblende) from the surrounding granitic magma into small volumes of interstitial liquid that remain within the enclave.

Although the compositional range of the mafic and intermediate enclaves can best be explained by hybridization between a mafic magma and the CMG magma, there are many lines of evidence which indicate that most of this hybridization (chemical as well as mechanical) occurred at a remote location and that the

Downloaded from https://academic.oup.com/petrology/article-abstract/38/3/393/1564739
by Trinity University user
on 15 February 2018

Downloaded from https://academic.oup.com/petrology/article-abstract/38/3/393/1564739
by Trinity University user
on 15 February 2018

Table 2: Chemical analyses of medium-grained ('cumulate') rocks from the gabbro–diorite unit; for elements determined by more than one method, results by the most accurate method are reported

	E-F	EMS-4A	67Y	MS-13	MS-11	MS-17	10	M	49	46A	141	MS-14	127	EMS6F3	MS-18	MS-12	L59.5	L69.7
Major elements (wt %)																		
SiO_2	44·20	44·49	46·31	46·48	46·62	46·72	46·82	47·16	47·59	47·62	47·76	48·15	48·40	48·61	48·78	48·83	49·60	49·72
TiO_2	1·28	1·28	1·27	1·85	1·95	1·49	0·96	1·95	0·88	1·77	1·19	1·89	0·78	1·72	1·33	2·58	1·30	3·08
Al_2O_3	11·07	12·01	13·78	16·63	16·44	17·33	17·93	16·34	18·92	17·34	17·33	16·36	21·19	16·28	16·72	14·24	16·17	10·61
Fe_2O_3	3·67	13·24	2·05	11·47	11·85	10·48	1·95	2·71	2·28	2·49	2·19	11·30	2·07	12·00	9·88	11·26	1·29	2·13
FeO	8·93	n.a.	9·70	n.a.	n.a.	n.a.	6·78	8·28	5·38	8·14	6·63	n.a.	6·10	n.a.	n.a.	n.a.	7·34	12·40
MnO	0·20	0·19	0·19	0·17	0·18	0·16	0·15	0·18	0·12	0·18	0·14	0·18	0·12	0·17	0·16	0·18	0·16	0·29
MgO	17·99	16·88	12·89	7·98	7·82	8·53	10·29	8·13	7·97	7·00	8·32	6·96	5·31	7·00	7·23	5·83	7·35	7·79
CaO	7·65	8·47	8·72	9·84	10·04	10·46	11·36	10·27	12·64	11·01	11·04	9·76	11·30	8·88	9·42	11·12	10·22	7·61
Na_2O	1·51	1·79	2·56	2·82	2·98	2·86	2·56	2·72	2·36	2·58	2·83	3·10	2·33	3·28	2·92	3·41	2·65	1·66
K_2O	0·54	0·35	0·37	0·45	0·41	0·30	0·13	0·43	0·18	0·66	0·27	0·60	1·05	1·55	0·99	0·46	0·91	0·75
P_2O_5	0·22	0·21	0·17	0·30	0·32	0·22	0·10	0·31	0·07	0·26	0·07	0·29	0·05	0·29	0·20	0·43	0·21	0·72
LOI	2·67	2·60	1·24	1·78	0·56	0·68	1·57	1·93	1·42	1·78	2·44	1·23	2·48	1·24	1·27	0·70	1·80	3·89
Total	99·93	101·51	99·25	99·77	99·17	99·23	100·60	100·41	99·81	10·83	100·21	99·82	101·18	101·02	98·90	99·04	99·00	100·65
Trace elements (p.p.m.)																		
Ni	369	349	323	135	113	137	231	117	151	60	166	84	21	76	100	59	80	85
Sc	26	31	32	31	33	30	38	30	33	36	34	34	13	31	31	55	30	39
Cr	1150	917	911	256	252	214	256	264	224	165	189	155	39	128	183	237	205	112
Co	79	75	49	46	47	49	48	43	38	43	39	45	28	41	42	37	37	55
V	190	208	195	249	256	214	185	251	178	280	191	254	139	242	214	355	156	269
Rb	15	9	12	11	10	8	5	11	7	13	14	17	43	57	27	12	27	23
Sr	270	276	219	263	261	271	238	300	264	382	240	261	387	294	249	239	260	135
Ba	88	72	97	82	88	69	29	98	27	138	34	111	98	351	150	113	116	208
Y	23	22	29	28	30	23	26	34	19	30	28	30	15	36	26	47	31	70
Zr	89	77	108	134	139	109	65	138	40	100	75	151	34	145	133	202	88	360
Nb	3	4	3	7	7	5	2	5	1	5	1	6	2	6	6	8	4	17
Ga	12	14	15	18	18	17	15	18	15	18	16	19	19	18	17	21	17	19
Be	0·8	1	0·9	1·2	1·3	1·1	0·8	0·8	0·7	1·4	0·9	1·4	0·8	1·5	1·3	1·6	0·8	0·5
La	n.a.	n.a.	7·28	n.a.	n.a.	n.a.	3·19	n.a.	2·01	n.a.	n.a.	n.a.	n.a.	n.a.	n.a.	n.a.	n.a.	n.a.
Ce	21·4	19·0	17·6	17·0	25·0	22·0	9·0	23·8	5·9	30·2	14·5	29·0	10·6	31·0	29·0	23·0	22·6	79·7
Nd	n.a.	n.a.	11·3	n.a.	n.a.	n.a.	6·2	n.a.	4·4	n.a.	n.a.	n.a.	n.a.	n.a.	n.a.	n.a.	n.a.	n.a.
Sm	n.a.	n.a.	3·61	n.a.	n.a.	n.a.	2·31	n.a.	1·84	n.a.	n.a.	n.a.	n.a.	n.a.	n.a.	n.a.	n.a.	n.a.
Eu	n.a.	n.a.	1·17	n.a.	n.a.	n.a.	0·89	n.a.	0·79	n.a.	n.a.	n.a.	n.a.	n.a.	n.a.	n.a.	n.a.	n.a.
Tb	n.a.	n.a.	0·65	n.a.	n.a.	n.a.	0·54	n.a.	0·41	n.a.	n.a.	n.a.	n.a.	n.a.	n.a.	n.a.	n.a.	n.a.
Yb	1·90	1·60	2·43	2·70	3·10	2·20	2·33	2·80	1·58	2·30	1·90	3·40	0·30	2·90	2·60	4·40	2·60	6·00
Lu	n.a.	n.a.	0·36	n.a.	n.a.	n.a.	0·30	n.a.	0·21	n.a.	n.a.	n.a.	n.a.	n.a.	n.a.	n.a.	n.a.	n.a.
Cu	43	47	40	41	44	55	63	41	53	58	69	47	31	42	49	51	48	91
Zn	88	82	85	74	83	69	55	82	52	85	61	87	73	105	73	75	76	158
U	n.d.	n.d.	n.d.	n.d.	1·2	n.d.	2·2	n.d.	n.d.	n.d.	n.d.	0·8	0·8	0·7	0·3	n.d.	1·6	0·9
Th	n.d.	n.d.	n.d.	0·6	0·9	n.d.	0·0	n.d.	n.d.	n.d.	n.d.	0·6	n.d.	n.d.	2·7	3·2	n.d.	n.d.
Hf	n.a.	n.a.	2·5	n.a.	n.a.	n.a.	1·6	n.a.	1·2	n.a.	n.a.	n.a.	n.a.	n.a.	n.a.	n.a.	n.a.	n.a.
Ta	n.a.	n.a.	0·2	n.a.	n.a.	n.a.	0·1	n.a.	0·1	n.a.	n.a.	n.a.	n.a.	n.a.	n.a.	n.a.	n.a.	n.a.

Downloaded from https://academic.oup.com/petrology/article-abstract/38/3/393/1564739
by Trinity University user
on 15 February 2018

Table 2: continued

	MS-4	101A	103	MS-3	MS-5	2	MS-20	MS-22	L76·6	126C	41B	MS-23	MS-6	EMS-4F	MS-16	MS-9	126B	L71·7
Major elements (wt %)																		
SiO_2	49·96	50·58	52·28	52·97	53·77	54·66	55·57	55·64	55·87	55·90	55·92	56·02	56·14	56·45	56·53	56·82	56·83	57·06
TiO_2	3·07	1·00	1·10	2·08	1·79	1·78	1·85	1·69	1·94	1·62	1·94	1·65	1·59	1·46	2·07	1·63	1·75	1·40
Al_2O_3	11·54	19·15	18·47	13·63	16·71	15·32	17·15	16·02	16·18	18·37	16·82	15·98	18·12	16·16	15·70	16·02	15·58	17·72
Fe_2O_3	14·34	1·75	3·04	12·14	10·66	1·90	8·75	9·80	2·22	2·38	3·44	8·68	7·82	12·76	9·94	9·93	3·57	1·89
FeO	n.a.	7·65	6·90	n.a.	n.a.	9·44	n.a.	n.a.	6·46	5·15	5·76	n.a.	n.a.	n.a.	n.a.	n.a.	6·15	6·04
MnO	0·27	0·16	0·18	0·22	0·17	0·23	0·15	0·18	0·17	0·14	0·16	0·17	0·13	0·11	0·14	0·19	0·16	0·14
MgO	6·65	3·52	3·49	5·53	2·79	3·34	2·60	3·22	2·69	2·23	2·65	3·05	2·06	1·81	2·81	2·41	2·54	2·34
CaO	6·93	10·15	9·38	6·82	6·50	7·02	6·32	6·19	6·59	6·43	6·49	6·33	6·39	4·61	5·92	5·50	5·96	6·64
Na_2O	2·27	3·03	3·19	3·03	4·19	4·63	4·41	4·34	4·04	4·82	4·16	4·15	4·82	5·02	4·25	4·11	4·07	4·48
K_2O	1·16	0·50	0·80	0·98	1·32	0·87	1·23	1·34	1·26	0·71	1·12	1·42	1·17	1·06	1·00	1·60	1·05	1·32
P_2O_5	0·82	0·09	0·20	0·29	0·60	0·26	0·51	0·42	0·54	0·36	0·48	0·39	0·49	0·29	0·58	0·45	0·54	0·44
LOI	2·10	1·47	1·34	1·50	0·70	1·36	0·33	1·21	1·69	1·83	1·33	1·21	0·44	0·49	0·00	0·40	2·06	1·45
Total	99·11	99·05	100·37	99·19	99·20	100·81	98·87	100·05	99·65	99·94	100·27	99·05	99·17	100·22	98·94	99·06	100·26	100·92
Trace elements (p.p.m.)																		
Ni	72	16	8	54	14	7	16	26	13	11	12	17	10	13	15	16	7	8
Sc	33	30	29	31	23	28	17	23	23	14	17	20	17	16	19	19	20	20
Cr	102	10	14	76	10	2	12	56	24	22	9	31	6	26	14	16	7	4
Co	55	33	25	41	24	28	24	25	16	n.d.	34	17	20	16	16	22	n.d.	13
V	294	241	218	224	197	250	211	169	182	142	231	175	139	85	213	145	154	154
Rb	33	12	22	28	39	24	37	37	35	18	38	31	31	53	42	50	28	34
Sr	138	446	503	191	280	384	280	258	311	399	296	305	288	292	244	238	330	325
Ba	300	142	231	275	370	186	327	468	274	213	304	283	367	301	219	306	219	268
Y	64	20	26	45	46	45	37	38	81	41	43	35	61	72	51	57	59	47
Zr	376	31	60	402	381	173	344	548	258	573	362	209	420	1245	294	635	434	299
Nb	19	3	4	12	12	6	15	13	16	16	13	n.a.	16	11	20	17	13	9
Ga	18	21	21	19	24	22	23	22	24	24	23	n.a.	24	28	21	22	24	24
Be	1·3	1·4	1·4	1·6	1·9	1·6	2·0	1·9	1·7	1·2	1·9	1·1	2·1	1·6	2·5	1·8	1·2	1·6
La	38·0	n.a.	n.a.	23·0	28·0	n.a.	n.a.	n.a.	n.a.	n.a.	31·6	15·0	31·0	n.a.	n.a.	n.a.	n.a.	n.a.
Ce	89·0	20·0	34·1	52·0	63·0	41·5	66·0	62·0	94·6	72·1	63·4	35·0	71·0	97·0	68·0	77·0	77·4	71·4
Nd	49	n.a.	n.a.	28	34	n.a.	n.a.	n.a.	n.a.	n.a.	28·5	19	40	n.a.	n.a.	n.a.	n.a.	n.a.
Sm	12·00	n.a.	n.a.	6·80	8·40	n.a.	n.a.	n.a.	n.a.	n.a.	7·34	5·00	9·70	n.a.	n.a.	n.a.	n.a.	n.a.
Eu	2·60	n.a.	n.a.	1·90	2·50	n.a.	n.a.	n.a.	n.a.	n.a.	2·03	1·80	3·30	n.a.	n.a.	n.a.	n.a.	n.a.
Tb	1·60	n.a.	n.a.	1·20	n.a.	n.a.	n.a.	n.a.	n.a.	n.a.	1·15	0·80	1·50	n.a.	n.a.	n.a.	n.a.	n.a.
Yb	5·80	n.a.	2·00	4·90	4·10	3·80	3·70	4·60	6·90	3·70	4·04	3·90	5·40	7·40	5·20	5·80	5·20	4·00
Lu	0·90	n.a.	n.a.	0·70	0·60	n.a.	n.a.	n.a.	n.a.	n.a.	0·60	0·50	0·80	n.a.	n.a.	n.a.	n.a.	n.a.
Cu	82	37	19	44	23	36	26	30	20	12	26	n.a.	13	35	40	16	17	18
Zn	137	83	87	120	95	136	83	97	92	81	92	n.a.	79	66	84	92	92	82
U	2·5	n.d.	1·1	1·5	2·9	n.d.	2·9	1·6	1·1	1·6	2·3	0·8	3·6	3·6	1·3	3·2	4·3	1·5
Th	6·5	n.d.	n.d.	4·6	5·9	0·8	6·7	6·4	7·5	0·5	1·9	2·1	8·4	4·6	8·6	9·4	4·3	1·7
Hf	8·8	n.a.	n.a.	8·6	9·3	n.a.	n.a.	n.a.	n.a.	n.a.	8·8	4·2	9·0	n.a.	n.a.	n.a.	n.a.	n.a.
Ta	2·0	n.a.	n.a.	0·5	0·5	n.a.	n.a.	n.a.	n.a.	n.a.	1·2	0·5	0·5	n.a.	n.a.	n.a.	n.a.	n.a.

Downloaded from https://academic.oup.com/petrology/article-abstract/38/3/393/1564739
by Trinity University user
on 15 February 2018

Table 2: continued

	117C	44B	EMS-4G	9	EMS6F2	EMS-4E	EMS-2A	MS-25	EMS-3B	EMS6F1	EMS-6D	32D	65B	39	43B	EMS-5A	EMS-5B	110B
Major elements (wt%)																		
SiO_2	66·40	57·75	59·32	59·81	60·46	61·17	61·34	61·51	61·84	62·33	62·43	62·58	63·17	64·71	64·95	65·11	65·12	65·85
TiO_2	0·92	1·45	1·31	1·22	0·88	0·71	0·76	0·95	0·66	0·68	0·79	0·76	0·99	0·74	0·72	0·56	0·64	0·69
Al_2O_3	13·36	15·96	16·59	15·38	19·89	20·29	17·60	15·02	18·62	19·01	18·75	14·82	15·77	16·93	16·54	18·01	18·55	14·31
Fe_2O_3	2·46	5·65	8·85	1·86	4·48	2·41	5·90	6·98	3·65	3·05	3·80	1·60	1·03	2·12	2·51	2·39	2·77	1·35
FeO	3·57	5·90	n.a.	5·26	n.a.	n.a.	n.a.	n.a.	n.a.	n.a.	n.a.	4·29	4·08	2·89	2·82	n.a.	n.a.	3·44
MnO	0·09	0·09	0·10	0·13	0·08	0·03	0·03	0·12	0·04	0·04	0·06	0·11	0·08	0·06	0·09	0·02	0·03	0·09
MgO	1·45	1·61	3·24	3·59	1·16	0·55	1·36	3·75	0·55	0·57	0·69	3·63	3·03	1·11	1·02	0·52	0·47	2·43
CaO	3·30	4·23	4·10	5·72	3·81	4·31	4·38	5·00	2·60	2·77	2·78	5·26	4·64	3·50	3·37	2·85	2·42	4·01
Na_2O	4·20	4·41	4·44	3·50	6·63	6·83	5·20	3·75	5·13	5·84	5·92	3·94	4·22	4·77	4·62	4·52	4·35	3·37
K_2O	2·37	1·30	2·40	2·35	2·29	1·13	1·22	1·46	4·61	3·80	3·66	1·33	1·86	2·25	2·60	3·97	5·36	3·35
P_2O_5	0·22	0·28	0·25	0·13	0·12	0·08	0·21	0·22	0·07	0·08	0·10	0·13	0·09	0·14	0·15	0·06	0·07	0·10
LOI	1·00	1·32	0·69	2·37	0·76	0·69	0·69	1·05	0·51	0·26	0·42	1·27	1·35	1·03	0·93	0·35	0·44	1·28
Total	99·34	99·95	101·29	101·32	100·56	98·20	98·69	99·81	98·28	98·43	99·40	99·72	100·31	100·25	100·32	98·36	100·22	100·27
Trace elements (p.p.m.)																		
Ni	10	12	18	14	8	6	14	58	3	3	5	60	46	8	10	3	3	26
Sc	14	12	15	26	6	2	5	14	4	4	5	16	16	6	9·5	3	3	14
Cr	12	19	37	21	14	19	13	106	n.d.	12	8	172	60	13	27	4	9	47
Co	17	15	23	24	10	6	13	25	8	8	8	22	16	6	9	8	8	24
V	73	92	152	177	57	34	105	89	28	36	42	119	99	68	56	35	32	97
Rb	61	68	115	107	48	39	55	50	93	65	85	66	55	90	79	85	100	119
Sr	178	293	265	258	300	381	344	243	293	284	267	248	170	237	246	304	293	127
Ba	511	359	970	248	2470	951	272	316	5530	4530	3240	610	857	591	585	3660	4860	352
Y	71	60	30	39	26	15	20	37	19	23	23	43	30	34	44	18	20	41
Zr	526	1356	146	104	522	407	646	301	449	520	569	207	147	553	598	391	475	169
Nb	15	12	15	6	11	8	7	10	11	10	12	8	9	11	11	8	10	8
Ga	22	27	21	17	22	21	22	17	20	21	21	18	17	23	22	18	18	16
Be	2·3	0·4	1·9	2·0	1·6	1·9	1·8	1·8	1·2	1·4	1·4	1·9	1·6	1·9	1·8	1·3	1·1	2·2
La	34·70	n.a.	n.a.	n.a.	n.a.	n.a.	n.a.	n.a.	n.a.	n.a.	n.a.	n.a.	n.a.	n.a.	n.a.	n.a.	n.a.	n.a.
Ce	74·5	79·2	48·0	41·8	48·0	24·0	46·0	65·0	38·0	33·0	40·0	61·9	42·6	82·8	133·2	36·0	36·0	64·0
Nd	40	n.a.	n.a.	n.a.	n.a.	n.a.	n.a.	n.a.	n.a.	n.a.	n.a.	n.a.	n.a.	n.a.	n.a.	n.a.	n.a.	n.a.
Sm	11·49	n.a.	n.a.	n.a.	n.a.	n.a.	n.a.	n.a.	n.a.	n.a.	n.a.	n.a.	n.a.	n.a.	n.a.	n.a.	n.a.	n.a.
Eu	2·34	n.a.	n.a.	n.a.	n.a.	n.a.	n.a.	n.a.	n.a.	n.a.	n.a.	n.a.	n.a.	n.a.	n.a.	n.a.	n.a.	n.a.
Tb	1·94	n.a.	n.a.	n.a.	n.a.	n.a.	n.a.	n.a.	n.a.	n.a.	n.a.	n.a.	n.a.	n.a.	n.a.	n.a.	n.a.	n.a.
Yb	6·86	6·10	2·60	3·65	2·80	1·40	2·30	3·90	2·00	2·50	2·20	4·00	3·30	3·80	4·48	2·00	2·00	4·10
Lu	0·97	n.a.	n.a.	n.a.	n.a.	n.a.	n.a.	n.a.	n.a.	n.a.	n.a.	n.a.	n.a.	n.a.	n.a.	n.a.	n.a.	n.a.
Cu	8	126	16	30	8	3	29	18	4	5	8	12	23	7	21	13	3	15
Zn	77	65	83	67	48	25	31	65	33	35	45	58	47	55	58	24	24	45
U	2·1	5·6	0·8	2·1	1·5	1·6	3·3	2·2	1·2	1·3	1·5	2·5	1·4	2·0	1·8	1·3	2·1	37
Th	9·8	5·1	2·0	7·2	1·4	4·8	9·5	12·1	0·7	1·9	23	2·0	6·9	5·9	10·0	4·3	3·5	12·0
Hf	15·2	n.a.	n.a.	n.a.	n.a.	n.a.	n.a.	n.a.	n.a.	n.a.	n.a.	n.a.	n.a.	n.a.	n.a.	n.a.	n.a.	5·1
Ta	1·4	n.a.	n.a.	n.a.	n.a.	n.a.	n.a.	n.a.	n.a.	n.a.	n.a.	n.a.	n.a.	n.a.	n.a.	n.a.	n.a.	1·0

Table 2: continued

	115	EMS-6B	38B	EMS-6A	68X	6B	68	42A	32B
Major elements (wt %)									
SiO_2	66·71	68·21	68·22	70·04	72·54	72·69	73·06	73·08	74·58
TiO_2	1·05	0·63	0·69	0·56	0·38	0·42	0·42	0·33	0·36
Al_2O_3	14·74	14·23	14·12	13·67	13·66	13·86	13·26	13·14	13·07
Fe_2O_3	2·26	5·32	1·03	4·20	1·63	1·42	1·62	1·58	1·28
FeO	3·08	n.a.	2·82	n.a.	1·56	1·80	1·60	1·24	1·70
MnO	0·12	0·10	0·05	0·08	0·07	0·07	0·07	0·05	0·06
MgO	1·14	0·77	1·63	0·61	0·43	0·46	0·41	0·34	0·34
CaO	3·16	2·00	3·12	1·60	1·26	1·32	1·28	0·94	1·11
Na_2O	3·75	4·61	4·34	4·30	3·54	4·36	3·59	3·64	3·98
K_2O	3·53	3·04	0·77	4·05	4·82	4·40	4·50	4·64	3·99
P_2O_5	0·23	0·12	0·13	0·10	0·07	0·08	0·07	0·05	0·05
LOI	0·62	0·31	2·19	0·32	0·31	0·54	0·47	0·67	0·89
Total	100·39	99·34	99·11	99·53	100·27	101·42	100·35	99·70	101·41
Trace elements (p.p.m.)									
Ni	4	5	1·5	4	4	2	3	7	3
Sc	11	9	9·3	8	6	6	8	5·3	6
Cr	12	6	36	45	11	6	n.d.	7	8
Co	13	8	9	5	13	3	2	1	10
V	84	36	69	31	20	17	18	13	17
Rb	115	65	30	87	111	129	123	110	114
Sr	153	117	187	84	65	76	80	51	58
Ba	628	924	252	675	641	685	668	519	562
Y	47	50	22	73	66	76	54	51	70
Zr	257	496	207	467	348	392	336	244	372
Nb	10	12	8	15	15	17	12	12	18
Ga	18	22	16	21	20	22	18	19	21
Be	2·1	1·5	1·6	2·2	2·7	3·3	1·8	2·5	3·1
La	n.a.	n.a.	n.a.	n.a.	27·2	n.a.	n.a.	27·7	n.a.
Ce	72·8	82·0	77·2	102·0	91·2	113·0	101·9	99·1	104·2
Nd	n.a.	n.a.	n.a.	n.a.	33·4	n.a.	n.a.	29·7	n.a.
Sm	n.a.	n.a.	n.a.	n.a.	9·94	n.a.	n.a.	8·10	n.a.
Eu	n.a.	n.a.	n.a.	n.a.	1·66	n.a.	n.a.	1·24	n.a.
Tb	n.a.	n.a.	n.a.	n.a.	1·83	n.a.	n.a.	1·51	n.a.
Yb	4·30	4·20	2·24	6·90	6·99	7·90	4·93	5·74	7·50
Lu	n.a.	n.a.	n.a.	n.a.	0·96	n.a.	n.a.	0·80	n.a.
Cu	9	5	14	7	7	3	5	0	4
Zn	54	80	35	69	40	48	48	48	51
U	2·8	1·4	2·2	0·7	1·2	4·4	1·8	2·8	3·4
Th	6·1	4·0	10·0	7·9	9·6	14·5	10·3	18·5	11·1
Hf	n.a.	n.a.	n.a.	n.a.	10·4	n.a.	n.a.	9·7	n.a.
Ta	n.a.	n.a.	n.a.	n.a.	1·3	n.a.	n.a.	1·3	n.a.

n.a., not analyzed; n.d., not detected.

enclave compositions were not significantly affected by direct interactions with the enclosing host granite. First, nearly all individual enclaves have sharp boundaries and lack compositional or textural zoning related to their margins. The compositions of the core and rim of one enclave are essentially identical except for slightly higher

Downloaded from https://academic.oup.com/petrology/article-abstract/38/3/393/1564739
by Trinity University user
on 15 February 2018

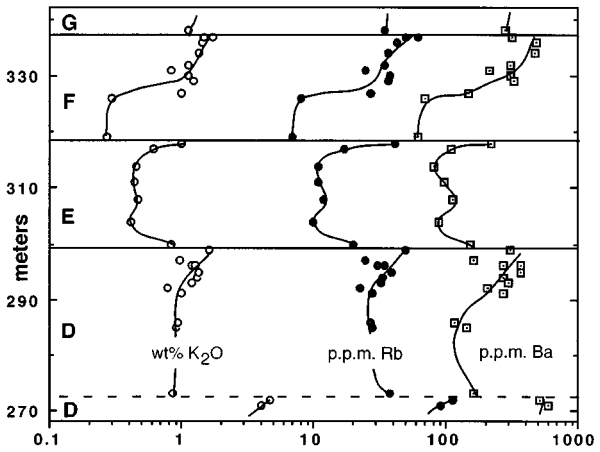

Fig. 7. Variation of K_2O, Rb, and Ba with respect to stratigraphic height (in meters) in the gabbro–diorite unit. Letters refer to the same units as shown in Fig. 2. Continuous horizontal lines represent the chilled gabbroic bases of prominent macrorhythmic units. Dashed line represents a chilled replenishment in unit D. It should be noted that the influx of new basaltic magma at the base of unit F only temporarily disrupts the trends of increasing K, Rb, and Ba, and that these elements reach much higher concentration in unit F than in unit E.

K_2O and Rb in the interior and Na_2O in the margin. Second, equilibrium between enclave and granite was not, in general, established because the mineralogy of enclaves at a given location is variable and commonly distinct from that of the host granite. Third, enclaves within the same outcrop commonly have very different chemical compositions, including alkalis (Fig. 9), even though they have similar SiO_2 contents and sizes, are unzoned, and occur in granite of homogeneous composition.

The fact that mafic and intermediate enclaves in the CMG occur within the same trends on Harker diagrams (Figs 4 and 5) strongly suggests that the mineralogy (e.g. clinopyroxene vs hornblende) is not a significant control on their chemical compositions. Most importantly, neither the chemical composition of the CMG magma nor the mineral assemblages of the enclaves can explain the high concentrations of incompatible elements of such different geochemical character (e.g. Yb, Be, Nb, Zn, Ga) within the enclaves. For example, there is no correlation between Y or Yb contents and the presence of amphibole (vs augite) in the enclaves. Furthermore, the host granite has a lower concentration than the enclaves in all of these elements, and the enclaves with the lowest SiO_2 are the most enriched.

Although exchange of alkalis and Sr-isotopes between enclave and host granite appears to be important in most settings (e.g. Holden *et al.*, 1991; Blundy & Sparks, 1992), there are some areas where even that type of exchange has been limited (Metcalf *et al.*, 1995). The relatively anhydrous character of the CMG may have reduced the potential for exchange of even these normally rapidly diffusing species between the upper CMG magma and its enclaves.

Possible sources of the enclaves

Because there are no known dikes with the mineralogy, textures and chemical compositions of the mafic enclaves, it seems most likely that they originated from magma that evolved within the CMG magma chamber. The great enrichment of many incompatible trace elements in these enclaves precludes generating their compositions by simple or even selective mixing with the CMG. Neither can these enclaves represent pieces torn from the G–D unit. Although enclaves have mineral assemblages that are similar to those of mafic diorites in the G–D unit, their textures and, more importantly, their chemical compositions are very different. Relative to G–D cumulates with comparable SiO_2, the chemical compositions of the mafic enclaves are greatly enriched in most incompatible trace elements (e.g. REEs, Nb, Be, and Ga) and depleted in compatible elements (e.g. CaO, MgO, Sr, and Ni) (Figs 4–6). The enclaves are characterized by strong negative Eu anomalies whereas the gabbroic to dioritic G–D cumulates have weak positive to negative Eu anomalies (Fig. 6). These compositional relationships suggest that the mafic (type 1) enclaves may closely resemble liquids (hybrid magmas?) that produced some of the G–D cumulates.

The dominant mineral assemblage of the intermediate enclaves (mesoperthite, clinopyroxene and Fe–Ti oxides) is unlike that of most of the CMG except for high-temperature cumulates near the shatter zone. These cumulates have abnormally low *mg*-number and normative An as do the enclaves, and they are similarly enriched in Mn, Na, Zn, and Ga, and depleted in V (Wiebe *et al.*, 1997). Therefore, these marginal cumulates provide support for the existence, at times, of magma broadly similar to these enclaves at depth within the CMG chamber. They differ, however, from the enclaves in having lower total REEs, positive Eu anomalies and higher Sr—a reflection of feldspar accumulation (Wiebe *et al.*, 1997). Liquids comparable with the type 2 enclaves could have produced the high-temperature cumulates near the shatter zone.

It seems most likely, therefore, that the mafic and intermediate enclaves formed from disrupted portions of compositionally stratified hybrid magmas that developed between mafic and silicic magmas near the base of the CMG chamber. Disruption of these basal magmas could be explained by fountaining of basaltic magma at the base of the CMG chamber, by earthquakes, or by episodes of eruption (of silicic magma from the upper part of the chamber) that temporarily disturbed the stable compositional stratification of magma in the chamber.

Downloaded from https://academic.oup.com/petrology/article-abstract/38/3/393/1564739
by Trinity University user
on 15 February 2018

Downloaded from https://academic.oup.com/petrology/article-abstract/38/3/393/1564739
by Trinity University user
on 15 February 2018

Table 3: Chemical compositions of magmatic enclaves in the Cadilla Mountain granite; for elements determined by more than one method, results by the most accurate method are reported

	182A	SI-4	182B	SI-14	S8-3	SI-3	1-10A	SI-17	SI-5(core)	SI-5(rim)	S2-2A	SI-6	SI-16	194C	S9-2A	91B	91AI
Locality:	HP	OC	HP	OC		OC	OC	OC	OC	OC	HS	OC	OC	SS			
Type:	1	1	1	1	1	1	1	1	1	2	2	2	2	2	2	2	2
Major elements (wt %)																	
SiO_2	55·66	58·39	59·70	59·72	59·94	60·36	60·72	60·93	61·17	61·95	62·16	62·60	62·94	63·34	64·00	64·58	64·98
TiO_2	1·32	1·19	1·11	0·96	0·98	0·94	0·91	0·84	1·01	0·96	1·10	0·59	0·74	0·49	0·68	0·62	0·66
Al_2O_3	14·02	14·15	13·85	14·67	15·34	14·52	14·84	14·66	14·06	14·28	14·07	15·40	15·06	14·41	13·48	15·72	15·47
Fe_2O_3	15·22	11·65	12·85	10·47	8·98	10·33	10·64	8·08	10·59	10·14	9·18	8·74	6·68	8·32	9·44	1·12	1·72
FeO	n.a.	n.a.	n.a.	n.a.	n.a.	n.a.	n.a.	n.a.	n.a.	n.a.	n.a.	n.a.	n.a.	n.a.	n.a.	3·06	3·25
MnO	0·43	0·32	0·35	0·32	0·29	0·32	0·37	0·32	0·40	0·40	0·29	0·28	0·24	0·20	0·27	0·16	0·19
MgO	1·28	1·11	0·99	0·96	1·12	0·96	0·87	1·06	0·95	0·86	1·07	0·69	0·86	0·52	1·10	0·81	0·85
CaO	4·25	4·49	3·24	3·75	3·37	3·42	3·00	4·43	2·97	2·62	3·58	2·37	2·92	2·56	3·11	2·54	2·70
Na_2O	6·03	5·16	6·16	6·14	5·07	6·19	7·24	6·28	6·35	6·81	5·04	7·19	6·20	7·41	6·02	5·78	5·71
K_2O	0·71	2·94	0·74	2·31	3·69	2·21	0·81	2·95	1·85	1·33	2·91	1·67	3·37	0·46	1·71	4·32	4·12
P_2O_5	0·35	0·36	0·31	0·29	0·34	0·21	0·24	0·28	0·29	0·25	0·34	0·17	0·23	0·10	0·11	0·15	0·18
LOI	1·48	0·47	1·66	0·64	0·87	0·96	1·17	0·48	0·84	1·22	0·58	0·93	1·05	0·90	0·40	0·64	0·90
Total	100·75	100·23	100·96	100·23	99·99	100·42	100·81	100·31	100·48	100·82	100·32	100·63	100·29	98·71	100·32	99·50	100·73
Trace elements (p.p.m.)																	
Ni	9	5	8	5	n.d.	n.d.	n.d.	5	5	n.d.	n.d.	4	n.d.	5	5	8	6
Sc	20	20	18	18	20	22	20	16	19	19	17	16	12	11	16	8	11
Cr	5	10	7	n.d.	6	17	10	9	12	14	n.d.	10	28	13	19	n.d.	n.d.
Co	6	9	6	9	9	6	10	7	7	7	10	8	8	4	11	3	4
V	56	37	46	29	33	36	30	56	37	33	43	19	45	22	61	27	27
Rb	60	79	75	65	133	62	33	93	70	56	116	61	91	49	64	122	120
Sr	83	94	60	89	91	74	67	67	66	65	92	68	52	38	62	94	71
Ba	189	493	206	422	566	553	305	618	484	436	317	507	618	161	260	959	903
Y	234	180	225	149	162	178	154	132	154	151	156	134	139	179	140	68	114
Zr	307	93	468	102	212	633	605	431	482	550	351	433	475	227	469	670	826
Nb	82	53	72	45	n.a.	n.a.	n.a.	31	53	n.a.	n.a.	28	n.a.	34	35	14	24
Ga	41	27	36	27	n.a.	n.a.	n.a.	24	26	n.a.	n.a.	27	n.a.	32	26	21	21
Be	14·2	5·6	14·4	5·2	10·2	4·2	5·4	2·4	5·8	4·5	9·9	4·2	3	7·7	13·4	1·9	2
La	79	41	44	50	60	30	50	41	30	31	35	86	71	37	32	40	n.a.
Ce	159·7	128	103	120	110	82	111	100	90	81	84	197	106	73·6	79	81·8	155
Nd	n.a.	86	n.a.	78	79	58	73	83	64	68	60	n.a.	90	n.a.	60	44·1	n.a.
Sm	n.a.	26·6	n.a.	22·9	22·6	19·7	21·5	23·3	20·7	18·8	18·4	n.a.	22·0	n.a.	19·1	12·4	n.a.
Eu	n.a.	3·4	n.a.	3·2	2·6	3·5	3·1	3·6	2·4	2·7	1·8	n.a.	3·2	n.a.	1·7	3·4	n.a.
Tb	n.a.	5·2	n.a.	4·3	4·3	4·2	4·0	4·1	4·2	4·0	3·9	n.a.	3·8	n.a.	3·8	1·9	n.a.
Yb	25·6	16·0	23·8	15·0	16·0	17·7	15·8	12·0	15·0	14·0	17·0	14·0	11·0	20·2	14·0	7·2	11·5
Lu	n.a.	2·4	n.a.	2·3	2·3	2·87	2·6	1·9	2·6	2·4	2·4	n.a.	1·7	n.a.	2·2	1·0	n.a.
Cu	9	2	9	2	n.a.	n.a.	n.a.	5	2	n.a.	n.a.	2	n.a.	13	3	5	3
Zn	315	226	279	228	n.a.	n.a.	n.a.	176	245	n.a.	n.a.	201	n.a.	120	178	112	146
U	8·9	2·7	7·4	4·6	2·0	3·9	2·0	1·8	3·6	3·0	5·0	2·8	2·0	3·9	2·6	2·0	2·4
Th	18·8	9·9	14·8	13·3	8·0	9·0	6·0	2·8	8·6	9·0	14·0	15·0	5·5	13·1	10·7	7·1	6·4
Hf	n.a.	4·4	n.a.	4·6	6·9	15·8	14·9	10·2	13·1	15·1	11·2	n.a.	11·5	n.a.	13·6	15·0	n.a.
Ta	n.a.	2·9	n.a.	2·7	2·9	2·9	2·4	1·5	2·9	2·9	3·5	n.a.	1·3	n.a.	2·1	1·1	n.a.

Table 3: continued

	SI-15	194D	160B	183B	182C	11B	11E	11D	169A	11C	11F
Locality:	OC	SS			HP	CMS	CMS	CMS	HS	CMS	CMS
Type:	2	2	2	2	2	3	3	3	3	3	3
Major elements (wt %)											
SiO_2	65·36	66·17	66·94	67·68	67·91	70·23	71·57	71·69	73·23	74·32	77·70
TiO_2	0·44	0·44	0·47	0·55	0·50	0·51	0·50	0·40	0·32	0·38	0·09
Al_2O_3	15·08	14·94	14·67	14·51	14·80	14·52	14·06	13·04	12·99	13·10	11·98
Fe_2O_3	7·14	5·67	5·23	3·80	4·83	0·86	0·97	1·59	3·30	0·94	0·70
FeO	n.a.	n.a.	n.a.	n.a.	n.a.	2·78	2·60	1·74	n.a.	2·94	0·86
MnO	0·18	0·15	0·16	0·25	0·17	0·14	0·13	0·19	0·07	0·18	0·05
MgO	0·37	0·39	0·43	0·38	0·36	0·58	0·50	0·26	0·21	0·35	0·01
CaO	1·19	1·75	1·31	1·79	2·13	1·30	1·15	0·53	1·11	0·51	0·11
Na_2O	6·29	4·68	4·91	4·52	7·96	5·09	4·75	4·34	4·81	4·54	3·20
K_2O	2·61	5·08	4·80	5·01	0·34	3·20	3·30	3·92	3·22	3·11	4·80
P_2O_5	0·09	0·10	0·09	0·15	0·10	0·09	0·06	0·03	0·05	0·03	0·00
LOI	1·89	0·66	0·70	1·73	1·21	1·74	1·50	1·19	0·39	1·30	0·84
Total	100·64	100·03	99·71	100·37	100·31	101·04	101·09	98·92	99·70	101·70	100·34
Trace elements (p.p.m.)											
Ni	n.d.	6	6	4	3	4	4	3	4	7	4
Sc	12	7	8	8	9	8	8	6	5	6	2
Cr	6	n.d.	n.d.	7	2	14	6	6	n.d.	12	3
Co	4	2	n.d.	5	n.d.	3	1	2	2	2	1
V	10	18	14	29	10	17	13	11	8	9	1
Rb	n.d.	179	165	159	42	119	121	129	120	87	175
Sr	63	36	46	33	59	131	114	65	63	36	13
Ba	542	528	631	606	271	607	614	767	673	589	279
Y	90	108	74	87	146	75	78	80	89	65	69
Zr	593	569	765	426	658	553	520	410	468	573	316
Nb	n.a.	29	28	21	38	19	19	18	22	20	24
Ga	n.a.	25	24	21	27	21	20	21	21	20	24
Be	2·1	8·9	2·9	2·5	6·6	5·1	4·7	3·5	3·7	0·9	3·8
La	21	29	48	50	18	59	36	73	57	21	33
Ce	53	62·2	89	92·9	60·7	106·7	89	145	115	69	104
Nd	n.a.	n.a.	n.a.	n.a.	n.a.	43·4	n.a.	n.a.	n.a.	n.a.	n.a.
Sm	n.a.	n.a.	n.a.	n.a.	n.a.	11·7	n.a.	n.a.	n.a.	n.a.	n.a.
Eu	n.a.	n.a.	n.a.	n.a.	n.a.	1·9	n.a.	n.a.	n.a.	n.a.	n.a.
Tb	n.a.	n.a.	n.a.	n.a.	n.a.	1·9	n.a.	n.a.	n.a.	n.a.	n.a.
Yb	9·5	13·3	9·2	9·4	16·3	8·0	8·7	8·3	9·3	7·3	9·1
Lu	n.a.	n.a.	n.a.	n.a.	n.a.	1·11	n.a.	n.a.	n.a.	n.a.	n.a.
Cu	n.a.	5	4	10	3	3	0	3	4	2	4
Zn	n.a.	131	120	581	305	93	89	101	67	100	57
U	n.a.	4·6	5·5	6·0	8·7	4·8	3·4	3·1	3·7	4·9	7·5
Th	n.a.	12·4	14·0	25·4	15·3	12·5	15·5	12·3	13·5	13·6	27·0
Hf	n.a.	n.a.	n.a.	n.a.	n.a.	22·0	n.a.	n.a.	n.a.	n.a.	n.a.
Ta	n.a.	n.a.	n.a.	n.a.	n.a.	1·6	n.a.	n.a.	n.a.	n.a.	n.a.

n.a., not analyzed; n.d., not detected.
Abbreviations: HP, Hadlock Pond; OC, Otter Cliffs Road; SS, Somes Sound; CMS, Cadillac Mtn. summit; HS, quarry near Mount Desert Island High School. (See Fig. 1.)

Downloaded from https://academic.oup.com/petrology/article-abstract/38/3/393/1564739
by Trinity University user
on 15 February 2018

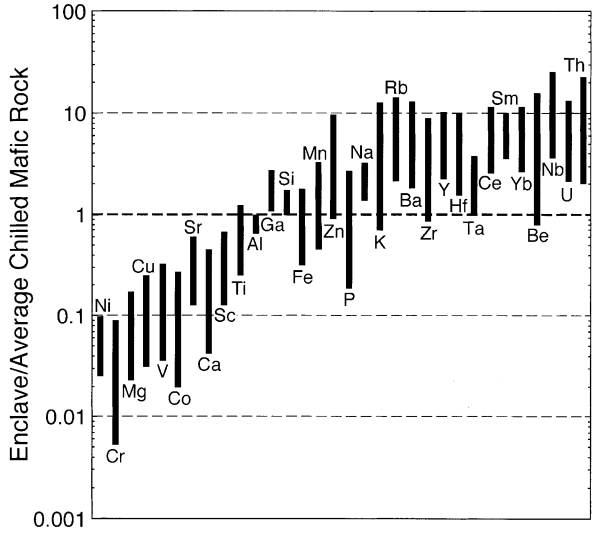

Fig. 8. Range of enclave compositions normalized to average chilled mafic rock (dikes and chilled margins in the gabbro–diorite unit).

The most silicic enclaves (type 3) have mineral assemblages and compositions that are comparable with those of typical upper CMG. They appear to be samples of liquids that evolved near the top of the chamber. These liquids were apparently disrupted by eruption through the roof of the magma chamber, leaving a trail of pressure-quenched globules in the partly crystallized solidification front beneath the roof (Wiebe & Adams, 1996).

Origin of the mafic end-member(s)

The enrichment of incompatible elements and depletion of compatible elements in type 1 enclaves are broadly consistent with extensive fractional crystallization from a basaltic magma. However, the enrichment in incompatible trace elements is much too great for simple closed-system fractional crystallization.

To produce this apparent decoupling of compatible and incompatible trace elements, it appears necessary to call upon multiple replenishments of basaltic magmas that mixed and underwent fractional crystallization (RFC) in a manner proposed by O'Hara & Mathews (1981) for mid-ocean ridge magma chambers. The stratigraphy of the gabbro–diorite unit strongly supports this model because it records hundreds of mafic replenishments. The process of decoupling would be most efficient if the basaltic magma cannot erupt out of the chamber. This appears to be the case when basaltic magmas are emplaced into silicic chambers. Many studies of silicic volcanic rocks have proposed that fractional crystallization of underlying mafic magmas played a major role in establishing strong compositional gradients of the source magma chambers (e.g. Ferriz & Mahood, 1987; Druitt & Bacon, 1988). Considerations of fractionation density (Sparks & Huppert, 1984) suggest that multiple replenishments could lead to the generation of more than one discrete compositional layer near the base of a silicic chamber.

Recharge–fractional crystallization (RFC) models

Equations presented by Reagan *et al.* (1987) were used to model the effects of simultaneous crystallization and intrusion on the composition of a liquid and to evaluate the feasibility of the replenishment–fractional crystallization (RFC) process. The equations were employed in a spreadsheet template that allows one to input the bulk distribution coefficient (D), ratios involving rates of intrusion (R_i), crystallization (R_c), and eruption (R_e), composition of the initial magma (C_o), and composition of replenishing magma (C_i). The results give the concentration of an element in the evolved liquid (C_{ev}) at numerous values of f (fraction of original magma left after crystallization) and F (ratio of final to initial mass of magma). An iterative approach was taken in calculating the effect of multiple replenishment and crystallization events on the evolving liquid. In the first cycle of each model, a mafic magma composition was input for C_i and allowed to evolve by pure fractional crystallization. The composition used for C_i is the average of the most primitive chilled mafic rocks (see Table 1; i.e. those with *mg*-number >0·60). After a certain amount of crystallization (e.g. 20%, $f = 0{\cdot}80$), the evolved liquid composition (C_{ev}) was re-entered as the composition of the original magma (C_o) which was replenished by and mixed with a fresh batch of basaltic magma (i.e. primitive mafic composition was input as C_i). The newly replenished–mixed magma crystallizes to some extent, and the process is repeated. Because the basaltic magma probably cannot erupt out of the chamber, R_i/R_c was set to a high value ($\sim 1{\cdot}0$) in all but the first cycle of the model (where $R_i/R_c = 0$), and $R_e/R_c = 0$ in all cycles. These conditions result in a magma chamber that remains nearly constant in volume (i.e. $F = 1{\cdot}0$).

Generalized results of the RFC modeling are illustrated in Fig. 10, where C_{ev}/C_o ratios are shown as a function of the number of RFC cycles for different D values. After a certain number of replenishments, the evolved liquid reaches a constant (or steady-state) composition ($C_{ev}/C_o = 1/D$) no matter how many more replenishments occur. For the conditions modeled here, the number of cycles that occur before the liquid reaching its steady-state composition is dependent on the D value. For compatible elements ($D > 1$), the steady-state composition is reached at a relatively low number (<15) of events.

Downloaded from https://academic.oup.com/petrology/article-abstract/38/3/393/1564739
by Trinity University user
on 15 February 2018

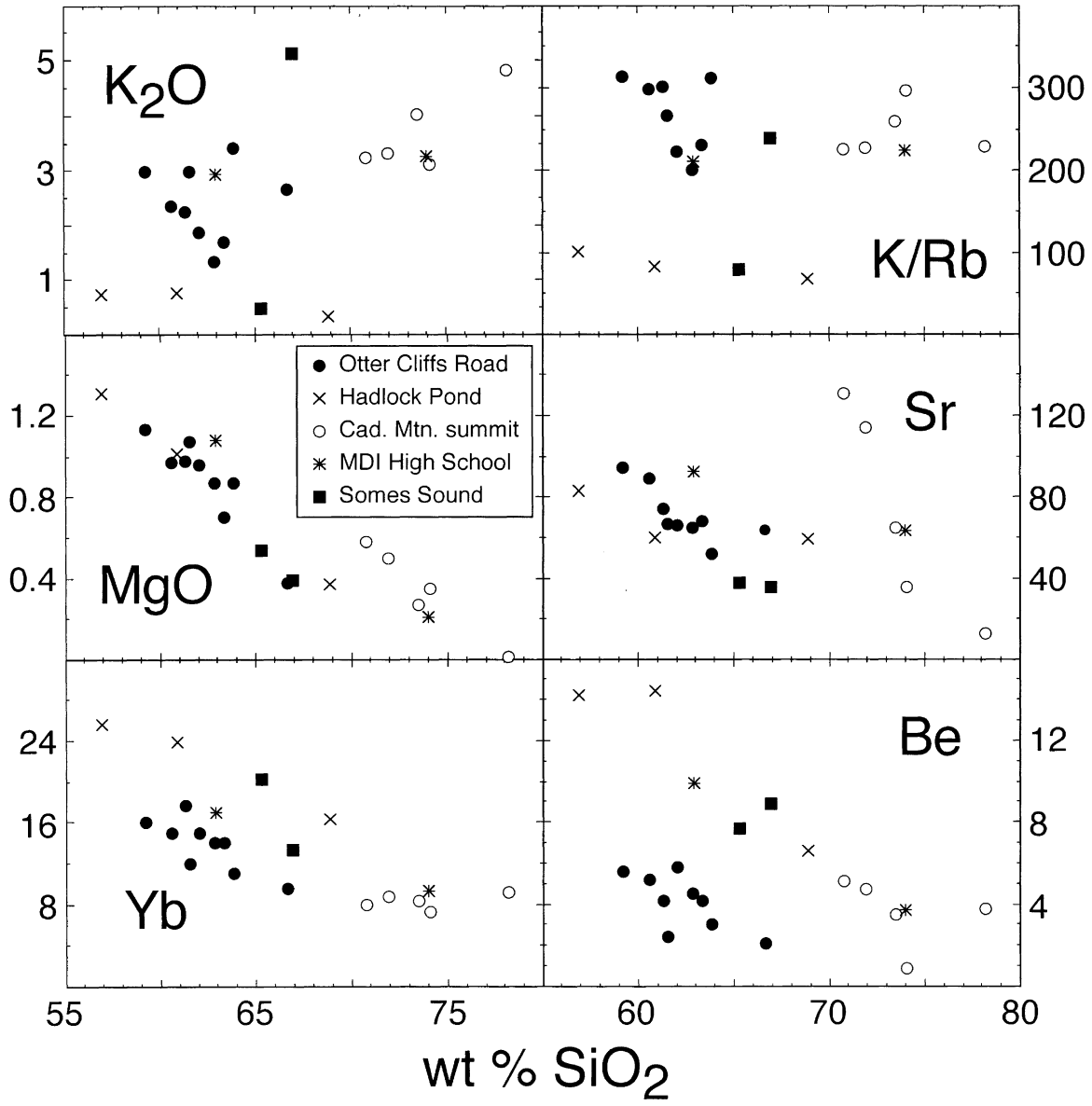

Fig. 9. Plots of enclave compositions subdivided so that enclaves from different outcrops have different symbols: SiO_2 vs K_2O, K/Rb, MgO, FeO_T, Be and Nb. (See Fig. 1 for locations of outcrops.)

Moderately incompatible elements (e.g. $D = 0{\cdot}5$) attain constant concentrations after ~30 replenishments, whereas strongly incompatible elements ($D \leq 0{\cdot}1$) do not reach constant compositions until >100 replenishments. The steady-state composition does not vary with the degree of crystallization before a replenishment–mixing event, but fewer events are needed for magmas that crystallize larger amounts before recharge (e.g. $f = 0{\cdot}60$ vs $0{\cdot}80$). An important consequence of these observations is that a magma that evolves via RFC processes becomes progressively enriched in strongly incompatible elements whereas moderately incompatible or compatible element abundances remain constant (O'Hara & Mathews, 1981).

Figures 11 and 12 illustrate RFC models developed in attempts to produce the compositions of the two least silicic enclaves, samples 182A and MS1–4. Models utilizing incompatible elements (Fig. 11) give generally good fits to the observed compositions. The D values used in the calculations are reasonable estimates for mineral assemblages (plagioclase, olivine, pyroxene, Fe–Ti oxides)

Downloaded from https://academic.oup.com/petrology/article-abstract/38/3/393/1564739
by Trinity University user
on 15 February 2018

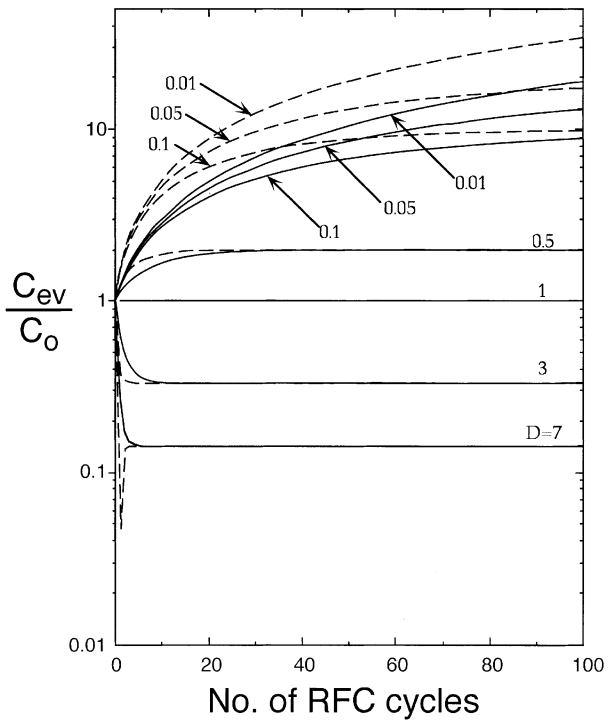

Fig. 10. Concentration in enclave magma over initial concentration (C_{ev}/C_o) evolved by RFC processes shown for different distribution coefficient (D) values; the ratios are plotted as a function of the number of RFC cycles. The first cycle in each model involves only fractional crystallization, but all subsequent cycles involve replenishment and mixing with fresh mafic magma, followed by some degree of fractional crystallization. For the dashed curves, $f = 0{\cdot}60$ (40% crystallization), and for the continuous curves, $f = 0{\cdot}80$ (20% crystallization). (See text for further discussion.)

likely to be crystallizing from mafic magmas. An exception is Zr, which appears to require small amounts (<0·05%) of zircon fractionation, especially in the generation of sample MS1–4. The models assume constant D values, but it is probable that they varied over time with changes in the specific mineral assemblage and modes. Only slight changes in D are required to bring the calculated curves closer to the observed compositions, and can be produced by small (and plausible) modifications in the fractionating assemblage. In addition, the models assume that the composition of the recharging magmas remained constant. A range of compositions of chilled mafic rocks from the CMIC is observed (Figs 3–5), thus it is likely that recharging magma compositions were not constant over time.

The number of RFC cycles required to generate the observed compositions can be estimated from models based on incompatible elements. The number required to generate sample MS1–4 (from the Otter Cliffs locality) is ~50, whereas a greater number (perhaps 150, or fewer if smaller D values are assumed) is required to produce sample 182A (from the Hadlock Pond locality). The stratigraphy of the gabbro–diorite units records hundreds of mafic replenishments, hence these numbers are plausible in light of field relations.

Figure 12 illustrates models based on compatible elements. In Fig. 12a, the D values used in the calculations are based on reasonable estimates of mineral assemblages crystallizing from basaltic magmas. The enclaves are significantly more depleted in the compatible elements than these models predict. Because compatible elements reach their steady-state composition after a relatively low number of replenishments, it is reasonable to assume that the sample/PCMR (primitive chilled mafic rocks) ratio equals $1/D$. Figure 12b illustrates models calculated using D values estimated with this approach. Obviously, the models provide good fits to observed enclave compositions, but the D values are unreasonably high. For example, D values for Ni and Co seem to require fractionation of only olivine ($\pm$ magnetite). In contrast, Sr seems to require fractionation of only plagioclase, and even then the D value is required to be 2·7 whereas K_D values for Sr in plagioclase in basaltic systems are generally assumed to be no higher than 2.

A possible explanation for these results may be that a magma evolved by RFC processes, and was then affected by pure fractional crystallization (FC) as a final step before its 'extraction' and emplacement as enclave material in the host granite. Figures 12c and 12d (and 11b) illustrate the effects of FC on a magma after it evolved through 100 RFC cycles. Better fits to the observed compositions are found, but only if somewhat high D values (especially for Sr and Sc) are employed. Involvement of oxides may explain V and Sc, but not Sr relationships. However, if the magma crystallized enough so that the residual liquid evolved to intermediate composition, an increase in the D values would be expected.

The RFC modeling is most realistic if thorough mixing can occur between evolved resident magma and the replenishing mafic magma. This is likely to be true as long as oxides are not cumulus phases and the resident magma is more dense than the replenishments (Sparks & Huppert, 1984). However, once fractionation of oxide phases begins, the density of the resident magma should decrease. When it is less than that of the replenishing mafic magma, incomplete mixing and magma stratification could result. In this case, the evolved intermediate magma would mainly be affected by fractional crystallization and could increase in volume as underlying replenishments underwent similar density reversals owing to the crystallization of oxides. The fact that most mafic enclaves are extremely depleted in V relative to the chilled mafic layers (parental magma) indicates that fractionation of oxides did occur.

Downloaded from https://academic.oup.com/petrology/article-abstract/38/3/393/1564739
by Trinity University user
on 15 February 2018

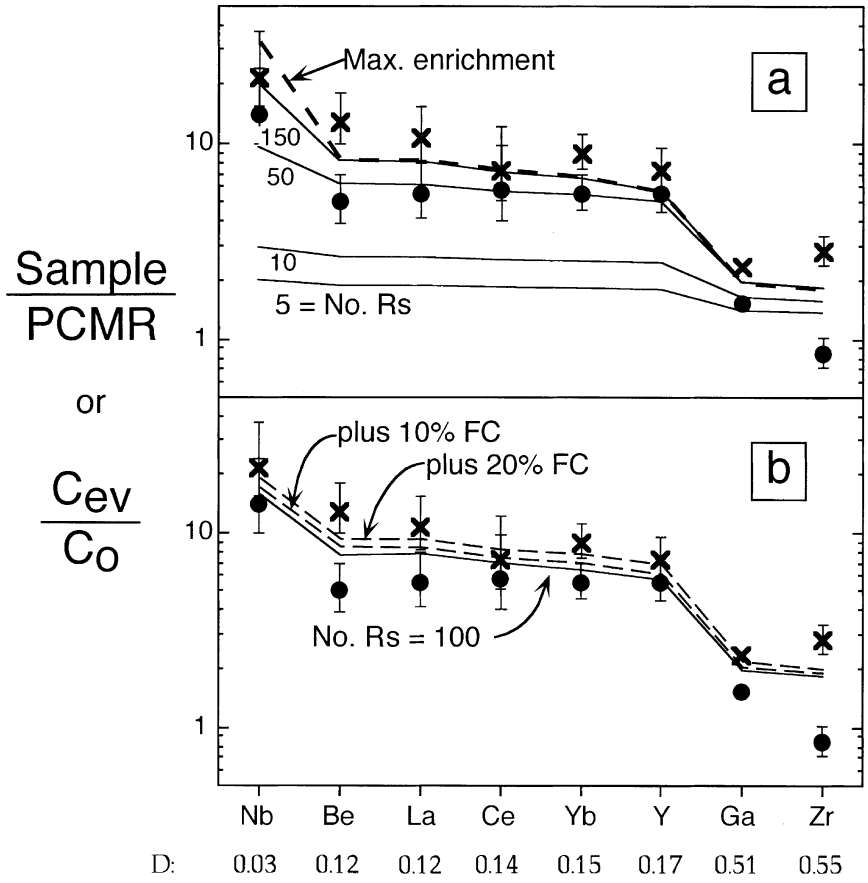

Fig. 11. (a) Concentrations of incompatible elements in two enclave samples (×, 182A; ●, MS1–4) divided by concentrations in the average of the most primitive (*mg*-number >0·60) chilled mafic rocks (PCMR). Error bars represent ranges in the normalized compositions when a range of PCMR compositions (1 SD) is used. Also shown are calculated C_{ev}/C_o ratios in liquids (continuous lines) evolved by RFC processes, where C_i is equal to the average PCMR, $R_i/R_c = 1{\cdot}0$, $R_e/R_c = 0$, and $f = 0{\cdot}80$ (20% crystallization before each replenishment and mixing). 'No. Rs' is the number of RFC cycles (see Fig. 10). Bulk distribution coefficients (D values) used in the calculations are listed for each element. The dashed line shows the maximum enrichment allowed for the selected D values. (b) Enclaves 182A and MS1–4 normalized to PCMR [symbols as in (a)], and C_{ev}/C_o ratios in a magma evolved by 100 RFC cycles [continuous line; same model parameters as in (a)] followed by pure FC (dashed lines; 10 and 20% crystallization).

If this explanation is true, then the magmas represented by the enclaves should have been in equilibrium with at least some of the intermediate cumulates within the gabbro–diorite unit. The large compositional variation shown by both the enclaves and rocks within the gabbro–diorite unit make it impossible, however, to establish a link between any specific cumulate and enclave. Nonetheless, in general, the mineral assemblages of the enclaves seem appropriate (e.g. early hornblende and biotite in the more mafic enclaves), and the gabbroic to mafic dioritic cumulates have, in a very broad sense, appropriate compositions to have been produced by magmas intermediate between normal basalt (the chills) and the most mafic enclaves. The isotopic compositions of the enclaves and the gabbro–diorites could provide support for the link, and these are the focus of planned future studies.

In situ *crystallization*

The effects of *in situ* crystallization resemble those of periodically replenished magma chambers (Langmuir, 1989). Compaction of crystalline mushes trapped beneath mafic replenishments could have caused filter pressing, which returned residual interstitial liquids from the crystalline mushes back into the liquid portions of the magma chamber. Field evidence for this process exists in the commonly occurring silicic pipes which extend upward

Downloaded from https://academic.oup.com/petrology/article-abstract/38/3/393/1564739
by Trinity University user
on 15 February 2018

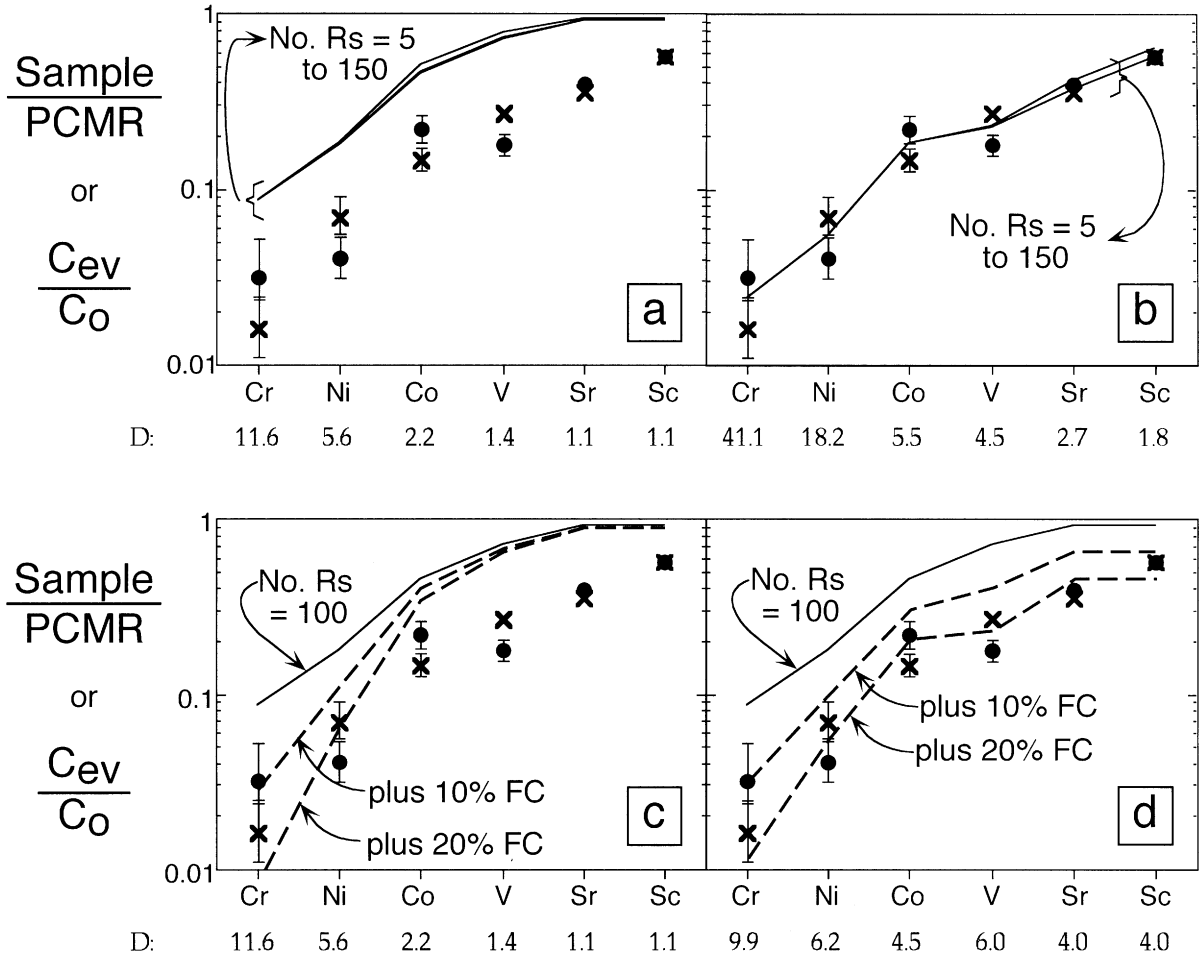

Fig. 12. (a) and (b), enclave samples 182A and MS1–4 normalized to PCMR [symbols and error bars as in Fig. 11(a)], and C_{ev}/C_o ratios (continuous lines) in magmas affected by 5–150 replenishment–mixing cycles [model parameters as for results shown in Fig. 11(a)]. (Note the 'compression' of the curves for 'No. Rs = 5–150' in contrast to the spread in Fig. 11.) *D* values used in the models illustrated in (a) were estimated from reasonable fractionating mineral assemblages, whereas the values used in (b) were estimated by assuming Sample/PCMR = 1/*D*. (c) and (d), enclaves 182A and MS1–4 [symbols and error bars as in Fig. 11(a)] and C_{ev}/C_o ratios in a magma evolved by 100 RFC cycles [continuous lines; model parameters as for results shown in Fig. 11(a)] followed by pure FC (dashed lines; 10 and 20% crystallization). *D* values used in (c) were estimated as in (a) above; *D* values used in (d) are those which provide good fits to the data.

from underlying silicic cumulates through the chilled bases of mafic replenishments (Wiebe, 1994). If the density of the filter-pressed liquid were between that of the basaltic and granitic magmas, then the filter-pressed liquid would also contribute to a growing intermediate layer. *In situ* crystallization and filter pressing might have operated in addition to RFC processes, thus reducing the number of replenishments required to produce a given level of enrichment.

Local variations in enclave compositions: implications for enclave dispersal

Although the compositions of enclaves are widely scattered on many plots of major and trace elements against SiO_2, a suite of enclaves from a restricted area commonly shows distinctive compositional features (e.g. unusually high Be, low K_2O, etc.) or very tight trends against SiO_2 for most elements (see Fig. 9). These distinctive local variations suggest that different enclave suites from restricted areas (within several tens of square meters) formed at different times from different events and involved discrete batches of intermediate magma. These 'events' probably involved eruption from the chamber, and one can view the enclaves as partially broken-up pieces of basal magma that were left behind within highly restricted volumes of the granite. This model of enclave formation conflicts with an earlier suggestion by Wiebe (1994) that enclaves in the upper CMG may have been distributed in a single major event and that their

Downloaded from https://academic.oup.com/petrology/article-abstract/38/3/393/1564739
by Trinity University user
on 15 February 2018

distribution provides evidence for whole body convection of the granitic magma.

A close examination of local variation in the sizes and abundances of enclaves also provides support for many localized events that affected only small volumes of the granite. Enclaves are not well size-sorted in any outcrops, nor is it apparent that different areas or elevations within the granite are characterized by systematic differences in average size. The abundance of enclaves appears to vary rapidly and randomly in many outcrops. The dispersal of enclaves probably occurred as many local 'blooms' which formed at different times rather than through wholesale convection of the chamber.

Tentative reconstructions of compositional gradients within the magma chamber

Because the CMG enclaves were almost certainly derived at different times from different hybrid magmatic layers near the base of the chamber, the compositional coherence within enclave suites from different localities in the CMG offers the opportunity to gain some insights into compositional stratification in the chamber. Three groups of enclaves shown in Fig. 9 are relevant. The Hadlock Pond (HP) and Otter Creek Road (OC) groups range in SiO_2 from ~58 to 66 wt % and probably sample liquids that evolved near the base of the chamber. The group of silicic enclaves from the near the summit of Cadillac Mountain (CMS) ranges from ~70 to 78 wt % SiO_2. This group appears to consist of quenched blobs of magma that were trapped during eruption (Wiebe & Adams, 1996) and may, therefore, preserve a record of compositional variation in the upper part of the chamber. Although all three groups show different ranges in SiO_2, they all have trends of decreasing TiO_2, FeO_T, MnO, MgO, CaO, P_2O_5, Sr, V, Sc, Zn, Y, and Yb with increasing SiO_2. If each group is a sample of different contemporaneous liquids, then the relative densities of these liquids require that all of those elements decrease upward in a compositionally stratified magma chamber.

Although the OC and HP groups have similar SiO_2, they are very different in the concentrations of many other elements (Fig. 9). On the basis of its occurrence deep within the intrusion, the HP group probably formed later than the OC group, which occurs close to the eastern margin of the granite. The HP group is characterized by especially high concentrations of Yb, Be, Nb, Zn, and Ga, all of which show decreasing abundances as SiO_2 increases. These high concentrations suggest that RFC processes produced highly enriched intermediate magmas late in the evolution of the magma chamber (i.e. after many, perhaps >100, RFC cycles), whereas magmas that were disrupted to form the earlier OC group had been affected by fewer replenishment events. The HP group is, however, distinct from the OC group in having very low abundances of K_2O and low K/Rb ratios. These differences are likely to reflect variable amounts of alkali exchange between mafic and silicic magmas within the chamber (Wiebe & Adams, 1996).

The high-SiO_2 group of enclaves from near the summit of Cadillac Mountain have apparently been quenched during eruption through the roof of the CMG magma chamber (Wiebe, 1996). They show very strong decreases in Al_2O_3, Na_2O, and Sr with increasing SiO_2, and increases in Rb and Nb. Compositional variation within this group of enclaves appears to be mainly controlled by feldspar fractionation. REEs in one of these enclaves have a pattern and abundances that closely match the CMG with the exception of a stronger than average negative Eu anomaly (Fig. 9). These relations indicate that the high-SiO_2 enclaves have undergone very little hybridization and that the compositional variation they show is largely related to feldspar fractionation in the upper portions of the silicic magma. They probably preserve a compositional stratification in the upper part of the magma chamber that was comparable with that shown in the Bishop Tuff (i.e. rhyolite from 70 to 78 wt % SiO_2) (Hildreth, 1979).

CONCLUSIONS

The origin of non-cumulate magmatic enclaves can be considered in the context of two end-members models: (1) direct break-up of new injections (e.g. dikes), and (2) disruption of evolving layers from the base of a compositionally stratified magma chamber. Enclaves formed in the first manner interact directly with the host granitic magma. If cooling is rapid, the only effective processes of hybridization should be those that are very rapid (e.g. alkali and Sr-isotope exchange); if cooling is very slow and temperatures remain above the solidus of the enclaves, more extensive exchange could occur. In either case, compositional variation within a group of these enclaves could point backward to the original compositions of the mafic injections (possibly preserved in associated mafic dikes).

For enclaves that originated through disruption of basal layers in the chamber, earlier processes of fractional crystallization, replenishment, and mixing may have been important, and much of the hybridization probably occurred remotely, e.g. at the interface between stably stratified mafic and silicic magmas near the base of the chamber. The compositions of these enclaves may vary widely under different circumstances depending upon many factors, including the rate of replenishment, the number of replenishment cycles, and the relative volumes of mafic and silicic magmas in the chamber. Fractional crystallization of the mafic input may be important, and

Downloaded from https://academic.oup.com/petrology/article-abstract/38/3/393/1564739
by Trinity University user
on 15 February 2018

the compositions of these enclaves should, in general, be very different from those of enclaves formed by direct interactions between mafic injections and resident silicic magma.

The enclaves in the Cadillac Mountain granite demonstrate that simple exchange between enclave and host granite may not always be a significant factor in determining the chemical compositions of enclaves. The ponding of mafic magmas at the base of granitic chambers and the development of compositionally stratified intermediate magmas will tend to preclude direct interactions between infusions of fresh basalt and resident granitic magma and yet provide an effective environment for the generation of evolved hybrid magmas (Bateman, 1995). This environment has been more widely considered a probable source of enclaves in volcanic rocks (e.g. Bacon & Metz, 1984; Grunder, 1994) than in plutonic rocks.

Many studies of enclaves have noted that enclave compositions are commonly enriched in 'incompatible' trace elements (e.g. Y, Yb, Nb). These high concentrations have been explained by diffusion from adjacent granitic magma to existing or growing crystals (e.g. hornblende, Fe–Ti oxides) in the enclave (Blundy & Sparks, 1992), so that enclave minerals are in equilibrium with the granitic melt and enclave compositions approach the compositions of mafic cumulates from the granite (Van der Laan & Wyllie, 1993). Although such an explanation may be correct, it is poorly constrained because it requires many assumptions about the percentage of liquid remaining in the enclave, rates of diffusion (not believed to be high for many of these elements), and distribution coefficients. For many of these enriched enclaves it is possible that remote processes have played a role in determining their compositions. Such high concentrations can be readily produced by RFC involving mafic replenishments at the base of a silicic magma chamber. In the case of the Mount Desert Island enclaves, there are also enrichments of many elements that cannot readily be attributed to diffusion between enclave and granitic host (e.g. Be, Ga).

The broad compositional scatter of enclaves within many granitic plutons has led some workers to question the significance of enclaves in the study of granite petrogenesis (Roberts & Clemens, 1995). Detailed sampling of enclaves in the CMG suggests, however, that compositional scatter may be greatly reduced by comparing enclaves from restricted areas. This spatial restriction of chemically distinct types of enclaves suggests both that enclaves formed at different times during the evolution of the granite and that the chemical character of the enclave sources also changed with time. A suite of enclaves from a small area, therefore, has the potential to provide an instantaneous record of magmas within the chamber and could lead to information about magma stratification in the chamber. Detailed sampling of enclaves in other granitic plutons could yield similar results.

ACKNOWLEDGEMENTS

We profited greatly from interactions in the field with the other Keck participants (Michelle Coombs, Sam Kozak, Naomi Lubick, Benjamin Plummer, Kathleen Schuh, Fred vanden Bergh, and Bud Wobus) as well as visitors to our project (Marshall Chapman, Dan Lux, Sheila Seaman, and Dave West). We are grateful to Steve Sylvester for assistance with analytical work at Franklin and Marshall College. The staff at Acadia National Park were helpful in many ways, and we are grateful to innumerable landowners who allowed us to tromp over their land. Reviews by T. P. Frost and P. Holden were very helpful, and we particularly appreciate a thorough and insightful review by A. L. Grunder. This research was supported by National Science Foundation Grants EAR-9003712 and 9204475 to R.A.W. In addition, during the summer of 1993, funds from The Keck Foundation, through the Keck Geology Consortium, provided additional support for several undergraduates and faculty from a total of seven colleges. D.S. acknowledges faculty development funds provided by Trinity University.

REFERENCES

Bacon, C. R., 1986. Magmatic inclusions in silicic and intermediate volcanic rocks. *Journal of Geophysical Research* **91,** 6091–6112.

Bacon, C. R. & Metz, J., 1984. Magmatic inclusions in rhyolites, contaminated basalts, and compositional zonation beneath the Coso volcanic field, California. *Contributions to Mineralogy and Petrology* **85,** 346–365.

Barbarin, B., 1991. Enclaves of the Mesozoic calc-alkaline granitoids of the Sierra Nevada Batholith, California. In: Didier, J. & Barbarin, B. (eds) *Enclaves and Granite Petrology. Developments in Petrology 13*. Amsterdam: Elsevier, pp. 135–153.

Bateman, R., 1995. The interplay between crystallization, replenishment and hybridization in large felsic magma chambers. *Earth-Science Reviews* **39,** 91–106.

Bedard, J., 1990. Enclaves from the A-type granite of the Megantic complex, White Mountain magma series: clues to granite magmagenesis. *Journal of Geophysical Research* **95,** 17797–17819.

Blundy, J. D. & Sparks, R. S. J., 1992. Petrogenesis of mafic inclusions in granitoids of the Adamello Massif, Italy. *Journal of Petrology* **33,** 1039–1104.

Bonin, B., 1991. The enclaves of alkaline anorogenic granites: an overview. In: Didier, J. & Barbarin, B. (eds) *Enclaves and Granite Petrology. Developments in Petrology 13*. Amsterdam: Elsevier, pp. 179–189.

Bussell, M. A., 1991. Enclaves in the Mesozoic and Cenozoic granitoids of the Peruvian Coastal Batholith. In: Didier, J. & Barbarin, B. (eds) *Enclaves and Granite Petrology. Developments in Petrology 13*. Amsterdam: Elsevier, pp. 155–166.

Downloaded from https://academic.oup.com/petrology/article-abstract/38/3/393/1564739
by Trinity University user
on 15 February 2018

Bussy, F., 1991. Enclaves of the Late Miocene Monte Capanne granite, Elba Island, Italy. In: Didier, J. & Barbarin, B. (eds) *Enclaves and Granite Petrology. Developments in Petrology 13*. Amsterdam: Elsevier, pp. 167–178.

Chapman, C. A., 1962. Bays-of-Maine igneous complex. *Geological Society of America Bulletin* **73,** 883–888.

Chapman, C. A., 1969. Oriented inclusions in granite—further evidence for floored magma chambers. *American Journal of Science* **267,** 988–998.

Chapman, M. & Rhodes, J. M., 1992. Composite layering in the Isle au Haut Igneous Complex, Maine: evidence for periodic invasion of a mafic magma into an evolving magma reservoir. *Journal of Volcanology and Geothermal Research* **51,** 41–60.

Coulon, C., Clocchiati, R., Maury, R. C. & Westercamp, D., 1984. Petrology of basaltic xenoliths in andesitic to dacitic host lavas from Martinique (Lesser Antilles): evidence for magma mixing. *Bulletin of Volcanology* **47,** 705–734.

Debon, F., 1991. Comparative major element chemistry in various 'microgranular enclave–plutonic host' pairs. In: Didier, J. & Barbarin, B. (eds) *Enclaves and Granite Petrology. Developments in Petrology 13*. Amsterdam: Elsevier, pp. 293–312.

Didier, J. & Barbarin, B. (eds), 1991. *Enclaves and Granite Petrology. Developments in Petrology, 13*. Amsterdam: Elsevier, 625 pp.

Dodge, F. C. W. & Kistler, R. W., 1990. Some additional observations on inclusions in the granitic rocks of the Sierra Nevada. *Journal of Geophysical Research* **95,** 17841–17848.

Druitt, T. H. & Bacon, C. R., 1988. Compositional zonation and cumulus processes in the Mount Mazama magma chamber, Crater Lake, Oregon. *Transactions of the Royal Society of Edinburgh: Earth Sciences* **79,** 289–297.

Ferriz, H. & Mahood, G. A., 1987. Strong compositional zonation in a silicic magmatic system: Los Humeros, Mexican Neovolcanic Belt. *Journal of Petrology* **28,** 171–209.

Frost, T. P. & Mahood, G. A., 1987. Field, chemical and physical constraints on mafic–felsic interaction in the Lamarck Granodiorite, Sierra Nevada, California. *Geological Society of America Bulletin* **99,** 272–291.

Furman, T. & Spera, F. J., 1985. Commingling of acid and basic magma with implications for the origin of I-type xenoliths: field and petrological relations of an unusual dike complex at Eagle Lake, Sequoia National Park, California, U.S.A. *Journal of Volcanology and Geothermal Research* **24,** 151–178.

Gilman, R. A., Chapman, C. A., Lowell, T. V. & Borns, H. W., Jr, 1988. *The Geology of Mount Desert Island. Maine Geological Survey, Bulletin* **38,** 50 pp.

Govindaraju, K., 1989. 1989 compilation of working values and sample description for 272 geostandards. *Geostandards Newsletter* **13,** Special Issue, 113 pp.

Grunder, A. L., 1994. Interaction of basalt and rhyolite in a bimodal suite. *Geological Society of America, Abstracts with Programs* **26,** A476–A477.

Hildreth, W., 1979. The Bishop Tuff: evidence for the origin of compositional zonation in silicic magma chambers. In: Chapin, C. E. & Elston, W. E. (eds) *Ash-Flow Tuffs. Geological Society of America, Special Paper* **180,** 43–75.

Hodge, D. S., Abbey, D. A., Harbin, M. A., Patterson, J. L., Ring, M. J. & Sweeney, J. F., 1982. Gravity studies of subsurface mass distributions of granitic rocks in Maine and New Hampshire. *American Journal of Science* **282,** 1289–1324.

Hogan, J. P. & Sinha, A. K., 1989. Compositional variation of plutonism in the coastal Maine magmatic province: mode of origin and tectonic setting: In: Tucker, R. D. & Marvinney, R. G. (eds) *Studies of Maine Geology: Igneous and Metamorphic Geology. Maine Geological Survey, Department of Conservation* **4,** 1–33.

Holden, P., Halliday, A. N. & Stephens, W. E., 1987. Neodymium and strontium isotope content of microdiorite enclaves points to mantle input into granitoid production. *Nature* **330,** 53–56.

Holden, P., Halliday, A. N., Stephens, W. E. & Henney, P. J., 1991. Chemical and isotopic evidence for major mass transfer between mafic enclaves and felsic magma. *Chemical Geology* **92,** 135–152.

Irvine, T. N., 1982. Terminology for layered intrusions. *Journal of Petrology* **23,** 127–162.

Johnston, A. D. & Wyllie, P. J., 1988. Interaction of granitic and basic magmas: experimental observations on contamination processes at 10 kbar with H_2O. *Contributions to Mineralogy and Petrology* **98,** 352–362.

Langmuir, C. H., 1989. Geochemical consequences of *in situ* crystallization. *Nature* **340,** 199–205.

Ludman, A., 1986. Timing of terrane accretion in eastern and east–central Maine. *Geology* **14,** 411–414.

Metcalf, R. V., Smith, E. I., Walker, J. D., Reed, R. C. & Gonzales, E. A., 1995. Isotopic disequilibrium among commingled hybrid magmas: evidence for a two-stage magma mixing–commingling process in the Mt. Perkins pluton, Arizona. *Journal of Geology* **103,** 509–527.

O'Hara, M. J. & Mathews, R. E., 1981. Geochemical evolution in an advancing, periodically replenished, periodically tapped, continuously fractionating magma chamber. *Journal of the Geological Society of London* **138,** 237–277.

Orsini, J., Cocirta, C. & Zorpi, M., 1991. Genesis of mafic microgranular enclaves through differentiation of basic magmas, mingling and chemical exchanges with their host granitoid magmas. In: Didier, J. & Barbarin, B. (eds) *Enclaves and Granite Petrology. Developments in Petrology 13*. Amsterdam: Elsevier, pp. 445–464.

Pitcher, W. S., 1991. Synplutonic dikes and mafic enclaves. In: Didier, J. & Barbarin, B. (eds) *Enclaves and Granite Petrology. Developments in Petrology 13*. Amsterdam: Elsevier, pp. 383–391.

Reagan, M. K., Gill, J. B., Malavassi, E. & Garcia, M. O., 1987. Changes in magma composition at Arental volcano, Costa Rica, 1968–1985: real-time monitoring of open-system differentiation. *Bulletin of Volcanology* **49,** 415–434.

Roberts, M. P. & Clemens, J. D., 1995. Are enclaves significant in granite petrogenesis? In: Brown, M. & Piccoli, P. M. (eds) *The Origin of Granites and Related Rocks. US Geological Survey Circular* **1129,** 127–128.

Seaman, S. J. & Ramsey, P. C., 1992. Effects of magma mingling in the granites of Mount Desert Island, Maine. *Journal of Geology* **100,** 395–409.

Seaman, S. J., Wobus, R. A., Wiebe, R. A., Lubick, N. & Bowring, S. A., 1995. Volcanic expression of bimodal magmatism: the Cranberry Island–Cadillac Mountain Complex, coastal Maine. *Journal of Geology* **103,** 301–311.

Sparks, R. S. J. & Huppert, H. E., 1984. Density changes during fractional crystallization of basaltic magmas: fluid dynamic implications. *Contributions to Mineralogy and Petrology* **85,** 300–309.

Sparks, R. S. J. & Marshall, L. A., 1986. Thermal and mechanical constraints on mixing between mafic and silicic magmas. *Journal of Volcanology and Geothermal Research* **29,** 99–124.

Stewart, D. B., Arth, J. A. & Flohr, M. J. K., 1988. Petrogenesis of the South Penobscot Intrusive Suite, Maine. *American Journal of Science* **288-A,** 75–114.

Stimac, J. A., Pearce, T. H., Donnelly-Nolan, J. M. & Hearn, B. C., Jr, 1990. The origin and implications of undercooled andesitic inclusions in rhyolites, Clear Lake Volcanics, California. *Journal of Geophysical Research* **95,** 17729–17746.

Taylor, T. R., Vogel, T. A. & Wilband, J. T., 1980. The composite dikes of Mount Desert Island, Maine: an example of coexisting acidic and basic magmas. *Journal of Geology* **88,** 433–444.

Downloaded from https://academic.oup.com/petrology/article-abstract/38/3/393/1564739
by Trinity University user
on 15 February 2018

Van der Laan, S. R. & Wyllie, P. J., 1993. Experimental interaction of granitic and basaltic magmas and implications for mafic enclaves. *Journal of Petrology* **34,** 491–517.

Vance, J. A., 1965. Zoning in igneous plagioclase: patchy zoning. *Journal of Geology* **73,** 636–651.

Vernon, R. H., 1983. Restite, xenoliths and microgranitoid enclaves in granites. *Journal and Proceedings, Royal Society of New South Wales* **116,** 77–103.

Vernon, R. H., 1984. Microgranitoid enclaves in granites—globules of hybrid magma quenched in a plutonic environment. *Nature* **309,** 438–439.

Vernon, R. H., 1990. Crystallization and hybridism in microgranitoid enclave magmas: microstructural evidence. *Journal of Geophysical Research* **95,** 17849–17859.

Watson, E. B. & Jurewicz, S. R., 1984. Behavior of alkalies during diffusive interaction of granitic xenoliths with basaltic magma. *Journal of Geology* **92,** 121–131.

Wiebe, R. A., 1973. Relations between coexisting basaltic and granitic magmas in a composite dike. *American Journal of Science* **273,** 130–151.

Wiebe, R. A., 1993*a*. Basaltic injections into floored silicic magma chambers. *Eos, Transactions of the American Geophysical Union* **74**(1), 3.

Wiebe, R. A., 1993*b*. The Pleasant Bay composite layered intrusion, coastal Maine: ponding and crystallization of basaltic injections into a silicic magma chamber. *Journal of Petrology* **34,** 461–489.

Wiebe, R. A., 1994. Silicic magma chambers as traps for basaltic magmas: the Cadillac Mountain intrusive complex, Mount Desert Island, Maine. *Journal of Geology* **102,** 423–437.

Wiebe, R. A., 1996. Mafic–silicic layered intrusions: the role of basaltic injections on magmatic processes and evolution in silicic magma chambers. *Transactions of the Royal Society of Edinburgh: Earth Sciences* **87,** .

Wiebe, R. A. & Adams, S. A., 1995. Enclave-rich zones in the Gouldsboro granite, Maine: a record of eruption and compositional stratification in a silicic magma chamber. In Brown, M. & Piccoli, P. M. (eds) *The Origin of Granites and Related Rocks. US Geological Survey Circular* **1129,** 165.

Wiebe, R. A., Holden, J. B., Coombs, M. L., Wobus, R. A., Schuh, K. J. & Plummer, B. P., 1997. The Cadillac Mountain intrusive complex, Maine: the role of shallow-level magma chamber processes in the generation of A-type granites. *Geological Society of America, Memoir* (in press).

Williams, H. & Hatcher, R. D., 1982. Suspect terranes and accretionary history of the Appalachian orogen. *Geology* **10,** 530–536.

Downloaded from https://academic.oup.com/petrology/article-abstract/38/3/393/1564739
by Trinity University user
on 15 February 2018